

# **Analysis of Boron Dilution Transients in a PWR**

**D.J. Diamond, B.P. Bromley, and A.L. Aronson**

**Nuclear Energy and Infrastructure Systems Division  
Energy Sciences and Technology Department  
Brookhaven National Laboratory  
Upton, New York, 11973**

**February, 2002**

**Prepared for  
U.S. Nuclear Regulatory Commission  
Washington, D.C. 20555**

## ABSTRACT

This report documents the results of three-dimensional coupled neutronics/thermal-hydraulics simulations of boron dilution events in a PWR following a small break loss of coolant accident. The coupled PARCS/RELAP5 code was used to model the Three Mile Island Unit 1 (TMI-1) PWR at beginning-of-cycle. A conservative plenum inlet boron concentration obtained from a simulation by Framatome Technologies was used as one of the key assumptions. Results demonstrated that the TMI-1 core would go prompt critical due to the boron dilution, reaching peak powers as high as 80% of nominal power, and causing fuel enthalpy to be as high as 37 cal/g in the hottest fuel pin near the bottom of the core in an unrodded low burnup fuel assembly near the reflector. Voids formed on a sporadic basis in channels with low flow rates or flow reversal, but the void fraction remained below 41%. The calculated fuel enthalpy was less than that obtained by Framatome Technologies using a more approximate model of the core. Nevertheless, the complex spatial behavior in the core, including the auto-catalytic increase in the natural circulation flow rate as power increases, makes it clear that three-dimensional models are important.

# CONTENTS

	<u>Page</u>
ABSTRACT .....	iii
ACKNOWLEDGMENTS .....	vi
LIST OF FIGURES .....	vii
LIST OF TABLES .....	ix
EXECUTIVE SUMMARY .....	x
1. INTRODUCTION .....	1
1.1 Background .....	1
1.2 Objectives .....	2
1.3 Outline of Report .....	2
2. CALCULATIONAL METHODOLOGY .....	3
2.1 PARCS Neutronics Code .....	3
2.2 RELAP5 Thermal-Hydraulics Code .....	3
2.3 PARCS/SA and PARCS/RELAP5 Models of TMI-1 PWR Core .....	3
2.4 Steady-State Rod Worth Calculations .....	9
2.5 Description of SBLOCA Preceding Boron Dilution Event .....	10
2.6 Boron Dilution Following Restart of Natural Circulation .....	11
2.7 Transient Analysis of Boron Dilution Events .....	11
3. DISCUSSION OF RESULTS .....	16
3.1 Transient Analysis with Boron Dilution - Case 1 .....	16
3.2 Transient Analysis with Boron Dilution - Case 2 .....	30
3.3 Comparisons with B&WOG Results .....	46
4. CONCLUSIONS AND RECOMMENDATIONS .....	48
5. REFERENCES .....	50

## ACKNOWLEDGMENTS

The authors wish to thank Dr. H. Joo of the Korean Atomic Energy Research Institute and Prof. T. Downar of Purdue University for their technical support in the use of the PARCS code and to Dr. J. Jo at Brookhaven National Laboratory for technical support in the use of the RELAP5 code. Thanks are also extended to Prof. K. Ivanov at Pennsylvania State University for providing the specifications and cross section data for the benchmark model of the TMI-1 PWR core. The authors also appreciate getting independent calculational results from Drs. A. Avvakumov and V. Malofeev at the Russian Research Centre - Kurchatov Institute, which helped assure the validity of the calculations done for this study. Finally, the authors thank Ms. S. Monteleone for assistance in the preparation of this report.

## LIST OF FIGURES

<u>Figure No.</u>	<u>Page</u>
2.1 Fuel Assembly Map Used by PARCS .....	5
2.2 Radial Arrangement of Control Rod Banks in TMI-1 Core .....	6
2.3 Thermal-hydraulic Channel Map Used by RELAP5 .....	7
2.4 RELAP5 Model of TMI-1 Core .....	8
2.5 Burnup Levels in TMI-1 Fuel Assemblies at BOC .....	9
2.6 Normalized Radial Power Distribution at BOC HZP .....	10
2.7 Boron Dilution Curves for B&W PWR .....	12
2.8 Boron Dilution Curves for TMI-1 Analysis .....	15
3.1.1 Power Variation in Case 1 .....	19
3.1.2 Logarithmic Power Variation in Case 1 .....	19
3.1.3 Total Reactivity Variation in Case 1 .....	20
3.1.4 Reactivity in Case 1 from 260 to 300s .....	20
3.1.5 Maximum Fuel Pellet Temperature in Case 1 .....	21
3.1.6 Maximum Fuel Pellet Enthalpy in Case 1 .....	21
3.1.7 Doppler and Moderator Reactivities in Case 1 .....	22
3.1.8 Boron and Control Reactivities in Case 1 .....	22
3.1.9 Core Average and Minimum Boron Concentration in Case 1 .....	23
3.1.10 Axial Power Distribution in Case 1 .....	23
3.1.11 Axial Power Distribution in Fa-151 (TH-27) in Case 1 .....	24
3.1.12 Assembly Averaged Radial Power Distribution at Time ~ 275 S in Case 1 .....	24
3.1.13 Radial Power Distribution in Axial Plane K=5 (Z=37 Cm) At Time ~ 275 S in Case 1 .....	25
3.1.14 Plane-Average Axial Boron Distribution in Case 1 .....	25
3.1.15 Axial Boron Distribution in Fa-151 (TH-27) in Case 1 .....	26
3.1.16 Assembly-averaged Radial Boron Distribution at Time ~ 277 S in Case 1 .....	26
3.1.17 Radial Power Distribution in Axial Plane K=5 (Z=37 Cm) at Time ~277 S in Case 1 .....	27
3.1.18 Assembly-Averaged Radial Coolant Density Distribution at Time ~ 277 s in Case 1 .....	27
3.1.19 Normalized Mass Flux Distribution in Case 1 at Time ~ 277 s at Inlet Junctions of Core (Mass Flux Average = 104.246 kg/m <sup>2</sup> /s, Total Flow Area = 5 m <sup>2</sup> ) .....	28
3.1.20 Normalized Mass Flux Distribution in Case 1 at Time ~ 277 s at Outlet Junctions of Core (Mass Flux Average = 119.87 kg/m <sup>2</sup> /s, Total Flow Area = 5 m <sup>2</sup> ) .....	28
3.1.21 Inlet Mass Flow in Channels TH-01, TH-07 and TH-09 in Case 1 .....	29
3.1.22 Inlet Mass Flow in Channels TH-20, TH-21 and TH-25 in Case 1 .....	29
3.2.1 Power Variation in Case 2 .....	33
3.2.2 Logarithmic Power Variation in Case 2 .....	33
3.2.3 Total Reactivity Variation in Case 2 .....	34
3.2.4 Reactivity in Case 2 at 240 to 340 s .....	34
3.2.5 Maximum Fuel Pellet Temperature in Case 2 .....	35
3.2.6 Maximum Fuel Pellet Enthalpy in Case 2 .....	35
3.2.7 Doppler and Moderator Reactivities in Case 2 .....	36
3.2.8 Boron and Control Reactivities in Case 2 .....	36
3.2.9 Core-Average and Minimum Boron Concentration in Case 2 .....	37

## LIST OF FIGURES (Cont'd)

<u>Figure No.</u>	<u>Page</u>
3.2.10 Maximum Void Fraction in Case 2 .....	37
3.2.11 Thermal-Hydraulic Channels with High Void in Case 2 .....	38
3.2.12 Axial Power Distribution in Case 2 .....	38
3.2.13 Axial Power Distribution in FA-137 (TH-23) in Case 2 .....	39
3.2.14 Assembly-Averaged Radial Power Distribution at Time ~ 259 s in Case 2 .....	39
3.2.15 Radial Power Distribution in Axial Plane k=3 (z=17 cm) at Time ~ 259 s in Case 2 .....	40
3.2.16 Plane-Average Axial Boron Distribution in Case 2 .....	40
3.2.17 Axial Boron Distribution in FA-137 (TH-23) in Case 2 .....	41
3.2.18 Assembly-Averaged Radial Boron Distribution at Time ~ 282 s in Case 2 .....	41
3.2.19 Radial Boron Distribution in Plane k=3 (z=17 cm) at Time ~ 282 s in Case 2 ..	42
3.2.20 Axial Void Distribution in FA-89 (TH-01) in Case 2 at Time ~ 282 s .....	42
3.2.21 Axial Void Distribution in FA-89 (TH-01) in Case 2 at Time ~ 292 s .....	43
3.2.22 Assembly Averaged Radial Coolant Density Distribution at Time ~ 282 s in Case 2 .....	43
3.2.23 Normalized Mass Flux Distribution in Case 2 at Time ~ 282 s at Inlet Junctions of Core (Mass Flux Average = 105.565 kg/m <sup>2</sup> /s, Total Flow Area = 5 m <sup>2</sup> ) .....	44
3.2.24 Normalized Mass Flux Distribution at Time ~ 282 s in Case 2 at Outlet Junctions of Core (Mass Flux Average = 117.525 kg/m <sup>2</sup> /s, Total Flow Area = 5 m <sup>2</sup> ) .....	44
3.2.25 Mass Flow in High-Void Channels TH-01, TH-07, TH-09 .....	45
3.2.26 Mass Flow in High-Void Channels TH-20, TH-25, TH-28 .....	45

## LIST OF TABLES

<u>Table No.</u>		<u>Page</u>
2.1	Specifications for the PARCS Neutronics Model of TMI-1 Core .....	4
2.2	Specifications for Thermal-Hydraulic Models of TMI-1 Core .....	4
2.3	Steady-State Rod Worth Calculations for TMI-1 at BOC, HZP .....	10
2.4	Conditions of B&W PWR Cores Before Dilution Transients .....	12
2.5	Initial Steady-State Conditions for PARCS/RELAP5 Model of TMI-1 .....	13
2.6	Flow Conditions Before Restart of Natural Circulation .....	14

## EXECUTIVE SUMMARY

A study was carried out to determine the response of a B&W reactor to boron dilution events as the result of a scenario initiated by a small break loss-of-coolant accident (LOCA). This scenario had been identified by the U.S. Nuclear Regulatory Commission (NRC) in Generic Safety Issue (GSI) 185, "Control of Recriticality following Small-Break LOCAs in PWRs." It was of concern due to the potential for a power surge and high enough fuel enthalpies to cause fuel damage. For high burnup fuel, fuel enthalpy limits may be lower than currently in effect. As part of the Task Action Plan generated by NRC to resolve the GSI, BNL has done calculations to compare with results generated for the B&W Owners' Group (B&WOG). The latter were done with more simple core analysis methods than those used at BNL, hence it was of interest to improve our understanding of the potential for unacceptable fuel damage and the effect of assumptions used in the analysis.

The event of interest starts with a SBLOCA of such size that in less than two minutes the reactor coolant system depressurizes, leading to loss of subcooling and boiling in the core. In response to the SBLOCA, the reactor is scrammed, and the reactor coolant pumps (RCPs) are tripped by the operator to slow the rate of losing coolant. After a period of approximately ten minutes, the high pressure injection system (HPI) is started, and borated water is pumped at a high flow rate into the pump discharge leg. Decay heat from the core is removed primarily by the steam generators operating in a high elevation boiler-condenser mode (BCM) and this causes the formation of deborated water condensate in the steam generators.

Within an hour, the high BCM process stops, and deborate formation in the steam generators is complete. Deborated water fills the steam generator and the pump suction pipe. Significant heat removal through the steam generators is no longer possible; therefore, the borated water from the HPI system continues to cool the core, and the flow from the small break will be a mixture of steam and water. After two to five hours, the core will have been cooled enough such that bulk boiling stops, and flow from the break transitions to a pure liquid phase.

The concern is that natural circulation can be reestablished during this period. Once natural circulation begins, the slug of deborated water in the steam generator is pushed through the pump suction pipe, discharge pipe, downcomer, and then into the lower inlet plenum. This slug of deborated water flowing through the core leads to a boron dilution event where recriticality of the core could occur.

The B&WOG analysis for this event had been based on the RELAP5 code with two thermal-hydraulic channels representing the active core and a point kinetics model. The calculation had assumed conservatively that the boron concentration throughout the core as a function of time was equal to that expected at the core inlet. The core inlet distribution was itself based on conservative analysis based on a model of the Crystal River Unit 3 reactor.

Two boron dilution transients were simulated by BNL. In one, the conservative inlet plenum boron concentration as a function of time was used based on the B&WOG analysis. In the other, the even more conservative boron reactivity assumption used by the B&WOG was simulated by changing the inlet boron concentration. A beginning-of-cycle core model of the TMI-1 B&W reactor was used with the coupled PARCS/RELAP5 neutronics/thermal-hydraulics code.

Due to limitations of the tabulated cross section data base used in the core neutronics model, the minimum moderator coolant temperature was restricted to 500 K. To maintain the same subcooling of the coolant at the lower inlet plenum during the boron dilution transient, the pressure during the transient was maintained at 15 MPa, instead of 6.6 MPa.

Simulation results demonstrated the complexity of the spatial effects during the event. The need for a three-dimensional neutron kinetics model for this analysis is clear. It is necessary to take into account the space-time dependence of the boron concentration, the auto-catalytic effect of increasing flow rate in assemblies with high powers, a core configuration with almost a checkerboard pattern of inserted control rods, and the moderator feedback from a complex thermal-hydraulics that may include reverse flow.

The boron dilution transients caused the core to go above prompt-critical, with peak reactivity and power as high as \$1.02 and 80% of nominal power, respectively. The peak enthalpy change in the fuel was found to be 16 and 37 cal/g in the two BNL simulations, which was 77 and 46% lower than the value obtained in the analysis by the B&WOG.

These fuel enthalpies are generally not larger than expected for the rod ejection accident (REA) in a PWR which is the design-basis accident for a PWR and for which NRC has an existing research program to understand fuel limits. Furthermore, the pulse widths for the boron dilution events are large compared with those expected for an REA and this is expected to have an ameliorating effect on fuel behavior.

The hottest fuel was found near the bottom of the core in low burn-up, unrodded, fuel assemblies near the reflector. Auto-catalytic behavior occurred where natural circulation forces drove more diluted water through the hotter channels, further increasing the localized relative power levels. For larger boron deficits, the power deposition in the fuel and heat transfer to the coolant were sufficient to cause significant void formation (over 40% void fraction). Competing reactivity effects of boron dilution vs moderator density and fuel temperature resulted in power oscillations that occurred over a period of 40 s. The power distributions and thermal-hydraulic conditions were such that no departure from nucleate boiling was expected.

The question of the potential for fuel damage due to departure from nucleate boiling in the boron dilution event may require a finer computational mesh for both the neutronic and thermal-hydraulic calculations, or perhaps even a fuel assembly sub-channel calculation. Since the current PARCS/RELAP5 model of the TMI-1 core does not permit cross-flow between fuel assemblies this adds to the uncertainty albeit probably so as to make the existing calculation conservative.

Another issue to consider is the time dependence of the boron concentration at the core inlet. The analysis done for the B&WOG was meant to be conservative although independent analysis has not verified this. The assumption that it is the reestablishment of natural circulation that causes the deborated slug to enter the core rather than restart of RCPs is based on operational safeguards in place at B&W plants. Additional calculations could be done to determine the parameters of the deborated slug of water (e.g., minimum boron concentration, rate of insertion, and total volume) which might lead to fuel enthalpies expected to be synonymous with fuel damage.

## 1. INTRODUCTION

### 1.1 Background

Boron dilution accidents in pressurized water reactors (PWRs) have been considered in many safety studies in the past. The concern has been to determine the probability of these beyond design-basis events, to simulate the neutronic and thermal-hydraulic behavior, i.e., to understand the consequences, and to address mitigating factors. The U.S. Nuclear Regulatory Commission has been concerned with these events and other reactivity initiated accidents especially because studies of high burnup fuel indicate that they may be susceptible to fuel failure at fuel enthalpies that were previously judged as acceptable.

One boron dilution scenario that has been considered in the past is initiated after a small-break loss-of-coolant accident (SBLOCA) when natural circulation is disrupted and reflux condensation allows deborated water to build up in the cold leg. Calculations supported by the B&W Owners' Group (B&WOG) [1,2] predicted prompt criticality with significant heat generation when natural circulation was reestablished. In light of this, the NRC wrote Generic Safety Issue (GSI) No. 185, Control of Recriticality Following Small-Break LOCAs in PWRs [3]

The calculations performed for the B&WOG were done (by Framatome Technologies) taking into account that under certain SBLOCA conditions with an interruption of the emergency core cooling system (ECCS), significant boiling of water in the core may occur. The resulting steam could then condense in the steam generator and a volume of distilled, deborated water would form in the cold leg of the coolant system. If natural circulation were reestablished or if the reactor coolant pumps were restarted to establish forced circulation again, a slug of deborated water would be pushed through the core, causing a reactivity excursion. Part of the analysis considered the potential for mixing of the deborated water with borated water in the cold leg, downcomer and lower plenum and part of the analysis was to see what were the consequences in terms of the core power if a particular slug of deborated water flowed through.

The NRC developed a task action plan [4] to resolve the GSI which included the calculation of the consequences in the core for the SBLOCA scenario. The previous computational analyses of this boron dilution event used zero-dimensional (point-kinetics) models coupled with transient thermal-hydraulic models. Static multi-dimensional few-group neutronics codes have been used to obtain axial and radial power shape functions and to calculate reactivity coefficients for use in the thermal-hydraulics and point-kinetics models. To get a more complete and accurate analysis of the dynamic behavior, it is advantageous to utilize a fully coupled three-dimensional, time-dependent neutronics/thermal-hydraulics model. This approach can give a better understanding of the potential for unacceptable fuel damage. This was the approach to be taken for the task action plan.

Brookhaven National Laboratory (BNL) has been tasked with the responsibility to do the analysis with the PARCS/RELAP5 code package. PARCS [5] provides the three-dimensional time-dependent neutronics calculation. It is coupled to RELAP5 [6] which provides the thermal-hydraulics analysis. The reactor model was based on the B&W plant, Three Mile Island Unit 1 (TMI-1) at beginning of a particular fuel cycle (BOC). This plant is similar, but not identical, to the Crystal River Unit 3 (CR-3) which was modeled in the B&WOG study.

## 1.2 Objectives

The work completed in this study had the following objectives:

- i) To compute steady-state conditions and neutronics parameters for a model of the TMI-1 PWR at BOC. These are to be compared against other calculations for validation of the model. .
- ii) To simulate two different boron dilution transient events using PARCS/RELAP5, a coupled, three-dimensional, time-dependent, neutronics/thermal-hydraulics model.
- iii) To evaluate the potential for fuel damage by boron dilution transients, as indicated by the maximum fuel enthalpy rise and departure from nucleate boiling ratio (DNBR) distributions.
- iv) To compare results of boron dilution transient analyses with those found earlier by the B&WOG.

## 1.3 Outline of Report

This report summarizes simulation studies of boron dilution events in a model of the TMI-1 PWR core at BOC using the coupled PARCS/RELAP5 neutronic/thermal-hydraulic codes. The computational model is described in Section 2, with steady-state calculations and comparisons with data provided by colleagues at the Russian Research Center - Kurchatov Institute. Also discussed in Section 2 are the input data for the boron dilution events. Presentation and discussion of results for two boron dilution events are given in Section 3 with comparisons to data from the earlier work reported on by the B&WOG. Conclusions and recommendations are given in Section 4.

## 2. CALCULATION METHODOLOGY

### 2.1 PARCS Neutronics Code

The PARCS (Purdue Advanced Reactor Core Simulator) code (Version v1.05) is used to simulate both the steady-state and transient reactor behavior of the TMI-1 PWR core model. PARCS is a three-dimensional, two-group diffusion model using nodal methods [5]. PARCS can be coupled with a thermal-hydraulics code such as RELAP5 to get a complete self-consistent simulation of the reactor core, or a simplified thermal-hydraulics model that is incorporated in the PARCS code can be used in a stand-alone mode. Although the stand-alone version of PARCS (PARCS/SA) has a limited range of applicability and accuracy, it can be run more quickly than the PARCS code coupled with RELAP5, and it is used in steady-state calculations to obtain individual rod worths and reactivity coefficients.

### 2.2 RELAP5 Thermal-Hydraulics Code

To model the temporal and spatial variation of the boron concentration during a PWR boron dilution event, it is necessary to use a thermal-hydraulics code such as RELAP5. RELAP5 [6] is a generalized thermal-hydraulics code developed for modeling light water reactors, or similar systems. Although the governing equations are essentially zero or one-dimensional, the three-dimensional thermal-hydraulic behavior in a reactor core can be modeled adequately by treating the core as an array of parallel one-dimensional flow channels and control volumes that are connected to each other by junctions at the inlet and outlet plena. The RELAP5 code can simulate reactor core behavior during a transient event by itself, utilizing a point kinetics model with input reactivity coefficients and relative power distributions. However, coupling RELAP5 directly to PARCS gives a direct and more comprehensive evaluation of the three-dimensional reactor neutronics feedback behavior and power deposition during a transient.

### 2.3 PARCS/SA and PARCS/RELAP5 Models of TMI-1 PWR Core

Several design and operational parameters of the TMI-1 PWR core model [7] and the discretization values used in the PARCS neutronics model are shown in Table 2.1. Parameters for the RELAP5 and PARCS/SA thermal-hydraulic models are shown in Table 2.2. There are 177 fuel assemblies (see Figure 2.1) and 64 reflector assemblies in the TMI-1 core. The PARCS model uses four neutronic nodes per fuel assembly/reflector, giving a total of 964 radial nodes. There are 28 axial neutronic nodes. The arrangement of all control rod banks in the TMI-1 core model [7] is shown in Figure 2.2. Banks 1, 2, 3, and 4 are safety banks that are inserted to shut down the reactor in the event of a reactor scram or a planned shut down. Banks 5, 6, and 7 are regulating banks that are used in conjunction with the boron chemical shim to adjust the power level and maintain criticality over the fuel life cycle. Bank 8 contains axial power-shaping rods (APSRs). Rods 7A, 7B, and 7C represent individual control banks of Group 7.

The version of PARCS in use for the analysis of the TMI-1 core makes use of a table look-up method for obtaining macroscopic cross section data for radially homogenized fuel assemblies. Data is available at various Doppler fuel temperatures, moderator densities, and boron concentrations within fuel assemblies of a specified composition of fissile and fertile isotopes, fission products, poisons, and with the presence (or absence) of a control rod. The core of the TMI-1 PWR is modeled with 438 different compositions for unrodded fuel assemblies, and 195 compositions for rodded fuel assemblies [7]. The cross section and assembly discontinuity factor data for each composition and energy group had been generated previously [8] by the

CASMO-3™ lattice physics code at the BOC burn-up levels for two values of boron concentration (5 ppm and 2000 ppm). The data structures of the tabulated cross section data at BOC required modifications to the subroutines in the PARCS sub-programs which are used for reading and interpolating/extrapolating data from the input cross section data files.

In the PARCS/SA thermal-hydraulics model, there is one radial node per fuel assembly, and the reflector assemblies are neglected; thus, there are 177 radial nodes, and 26 axial thermal-hydraulic nodes. The PARCS/SA model is useful for problems where the boron concentration is uniform, and where most thermal-hydraulic parameters do not deviate significantly from normal steady state operating conditions. The shaded assemblies in Figure 2.1 are a symmetric octant of the core which can be used to reduce the computational effort in the RELAP5 model, as represented in Figure 2.3. The RELAP5 model represents the TMI-1 core as 30 parallel one-dimensional thermal-hydraulic channels joined by common mixing volumes at the inlet and exit, as shown in Figure 2.4. The bypass reflector assemblies are treated as a single channel. The RELAP-5 thermal-hydraulic model uses a smaller number of axial nodes for the core than the PARCS thermal-hydraulics model (24 instead of 26), but the axial reflectors and both the inlet and exit plena are represented explicitly. The 29 distinct fuel assemblies in the octant of the TMI-1 core are shown in Figure 2.5 with the burnup levels, and the index schemes for PARCS and RELAP5.

**Table 2.1 Specifications for the PARCS Neutronics Model of TMI-1 Core**

Fuel Cycle	BOC
Full Power Level	2772 MWth
HZP Power Level	1.0e-4 %
Number of Fuel Assemblies (FA)	177
Number of Reflector Assemblies	64
Fuel Assembly Width	21.811 cm
Fuel Assembly Pitch	21.811 cm
Active Core Height	357.12 cm
Thickness of Axial Reflector	21.811 cm
Thickness of Radial Reflector	21.811 cm
Position of Fully Inserted Control Rod Relative to Bottom of Reflector	36.225 cm
Step Size for Control Rods	0.353 cm
Delayed Neutron Fraction (Beta)	0.006323
Number of Delayed Groups	6
Boron Concentration	1700 ppm
Number of Radial Neutronic Nodes	4*(177+64) = 964
Number of Axial Neutronic Nodes	28 (26 core, 2 reflectors)
Initial Position for Banks 1 to 4	Withdrawn (971 steps)
Initial Position for Banks 5,6,7	Inserted (0 steps)
Initial Position for Bank 8 (APSR)	Partial (291.3 steps)

**Table 2.2 Specifications for Thermal-Hydraulic Models of TMI-1 Core**

Thermal-Hydraulic Model	Stand Alone	RELAP5
Initial Inlet Coolant Temperature	278 C	278 C
Initial Inlet Coolant Flow	89.522 kg/s per FA	17,374 kg/s
Initial Boron Concentration	1700 ppm	1700 ppm
Number of Radial TH Nodes	177 (core)	30 (29 core, 1 reflector)
Number of Axial TH Nodes	26 (core)	26 (24 core, 2 reflectors)

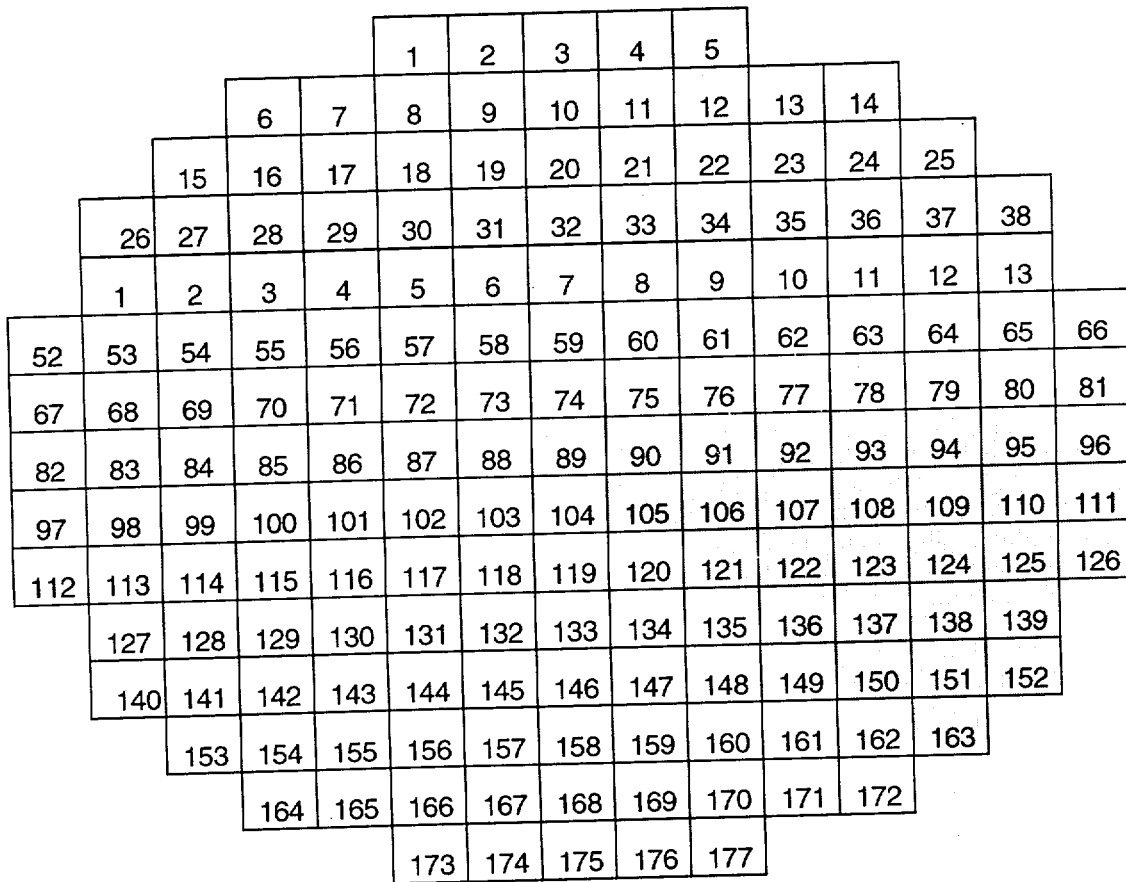


**Figure 2.1 Fuel Assembly Map Used by PARCS**

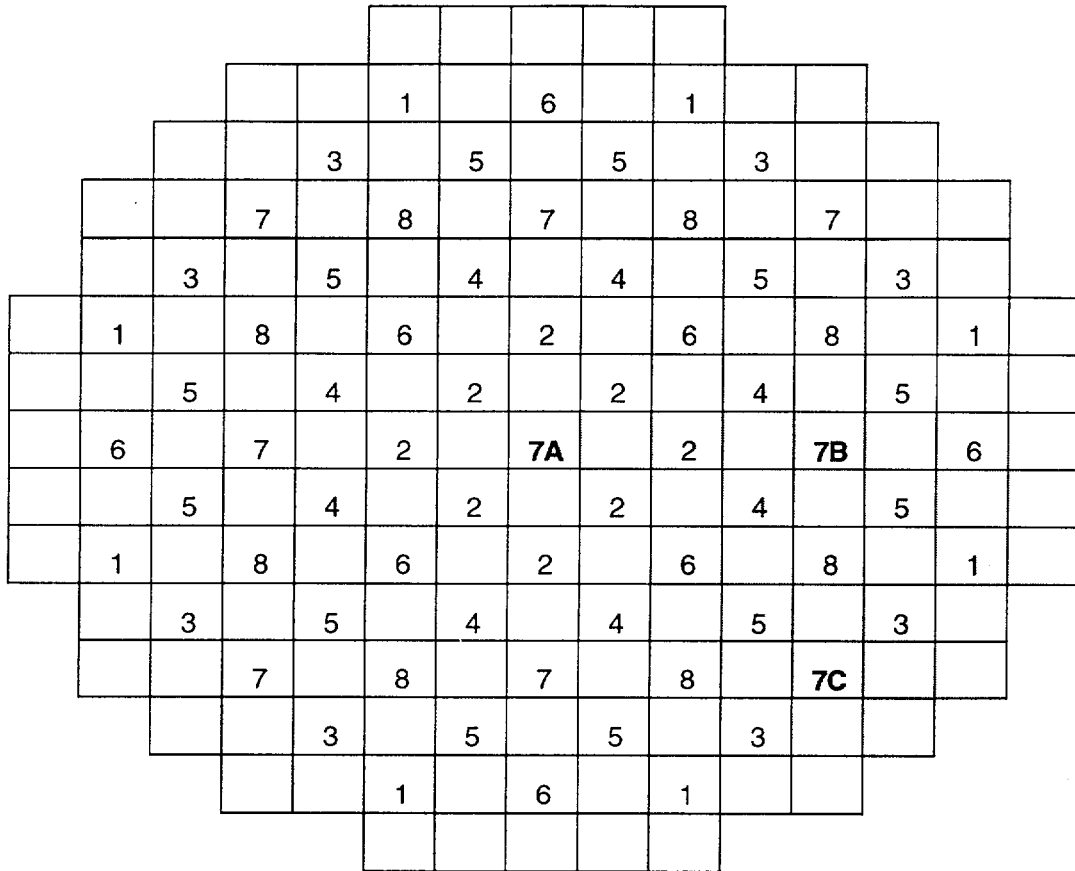
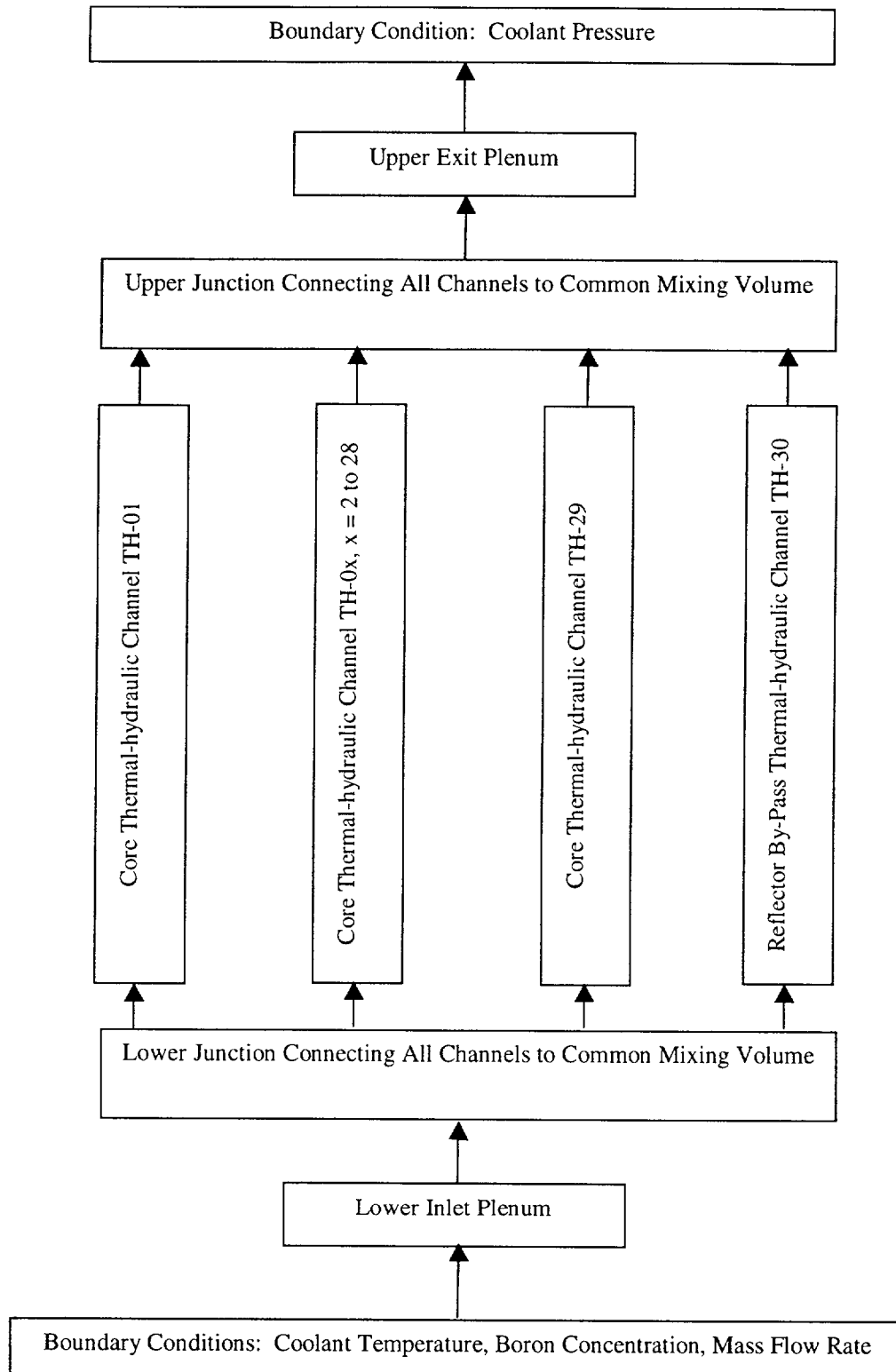


Figure 2.2 Radial Arrangement of Control Rod Banks in TMI-1 Core





**Figure 2.4 RELAP5 Model of TMI-1 Core**

1 89 30.69	2 90 0.16	3 91 29.50	4 92 0.18	5 93 24.53	6 94 0.16	7 95 36.51	8 96 48.20
	9 105 32.26	10 106 0.17	11 107 29.30	12 108 0.17	13 109 29.25	14 110 0.15	15 111 40.34
		16 121 31.69	17 122 0.18	18 123 30.12	19 124 0.17	20 125 0.14	21 126 39.62
			22 136 24.52	23 137 0.18	24 138 31.73	25 139 26.73	
				26 150 24.89	27 151 0.17	28 152 32.22	
					29 163 24.82		

TH Channel  
FA  
Burnup (GWD/T)

**Figure 2.5 Burnup Levels in TMI-1 Fuel Assemblies at BOC**

#### 2.4 Steady-State Rod Worth Calculations

The PARCS/SA code was used to compute the effective multiplication factor of the TMI-1 core at BOC in the steady-state condition at hot zero power (HZP) for various positions of control rod banks 5, 6, 7, and individual control rods 7A, 7B, and 7C. Safety banks 1 to 4 were fully withdrawn, while Bank 8 was inserted according to the specification given in Table 2.1. A reference steady state calculation was done first to obtain the effective multiplication factor when all control banks and individual rods (5, 6, and 7, including 7A, 7B, and 7C) are fully inserted. Steady-state calculations were then done with PARCS/SA to obtain the effective multiplication factor when an individual or group of control rod banks were fully withdrawn.

Steady-state calculation results with the PARCS/SA code for the control rod worths in the TMI-1 core at BOC, HZP are shown in Table 2.3 with comparisons to calculations done by colleagues at the Russian Research Center – Kurchatov Institute (RRC-KI) using the coupled BARS/RELAP5 code [9-11]. The BARS code uses a Green's Function approach based on multi-group diffusion equations to solve the neutron flux distributions on a pin-by-pin basis in the radial plane of a reactor core while a harmonic expansion is used to represent the flux in the axial direction. Nuclear data is generated with a companion code (TRIFON) taking into account the geometry and composition of all core fuel and non-fuel components.

As seen in Table 2.3, the PARCS/SA predictions for rod worths at BOC were found to be consistently less than those computed by BARS/RELAP5, differing from 2 to 12%. The control bank worths are within the expected uncertainties. Comparison of the normalized radial power distributions at BOC HZP with Banks 5, 6, and 7 inserted, as shown in Figure 2.6, does not appear to give any immediate physical explanation for the larger differences in the worths of individual control rods 7A, 7B, and 7C, although it is considered to be linked to the homogenized cross section data and assembly discontinuity factors for the fuel assemblies that

are adjacent to the reflector. It is possible that the pin-by-pin calculation done with BARS gives a more accurate representation of the flux variations in the fuel assemblies bordered by the reflector.

**Table 2.3 Steady-State Rod Worth Calculations for TMI-1 at BOC, HZP**

Rod / Bank	PARCS-SA Worth (pcm)	BARS/RELAP5 Worth (pcm)	Difference (%)
5	1247	1337	-6.7
6	723	761	-5.0
7	999	1026	-2.7
7a	245	276	-11.4
7b	149	166	-10.4
7c	473	519	-8.9

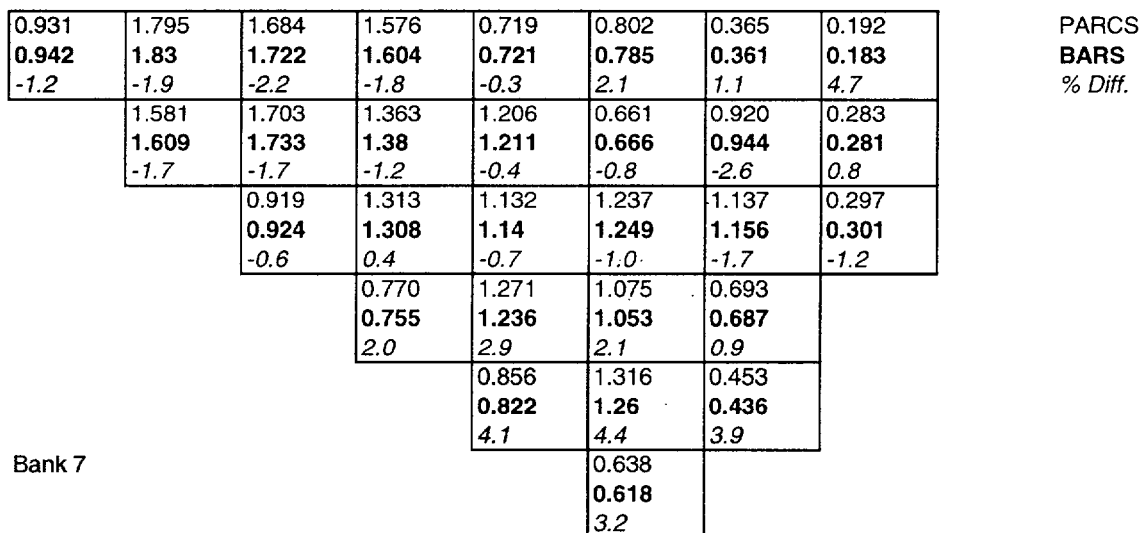


**Figure 2.6 Normalized Radial Power Distribution at BOC HZP**

### 2.5 Description of SBLOCA Preceding Boron Dilution Event

According to the previous analysis [1] for the B&WOG, small break loss of coolant accident (SBLOCA) in a PWR is an event where a coolant pipe breaks with a hole size ranging from 0.005 ft<sup>2</sup> to 0.05 ft<sup>2</sup> (4.6 cm<sup>2</sup> to 46 cm<sup>2</sup>). The coolant pipe may be connected to the main pump discharge/downcomer nozzle inlet, cold leg pump suction/steam generator exit, or the hot leg/steam generator inlet. In less than two minutes, an SBLOCA will cause the reactor coolant system (RCS) to depressurize, leading to loss of subcooling and boiling in the core. In response to the SBLOCA, the reactor is scrammed, and the reactor coolant pumps (RCPs) are tripped by the operator to slow the rate of losing coolant.

After a period of approximately ten minutes, the high pressure injection system (HPI) is started, and borated water is pumped at a high flow rate into the pump discharge cold leg so that it may enter the core through the nozzle inlet. Decay heat from the core is removed primarily by the steam generators operating in a high elevation boiler-condenser mode (BCM) and this causes the formation of deborated water condensate in the steam generators.

Within an hour, the high BCM process stops, and deborate formation in the steam generators is complete. Deboreted water fills the steam generator and the pump suction pipe. Although deboreted water can flow past the RCP into the pump discharge pipe, the flow rate is quite small in comparison to that of the highly borated water from the HPI pumps. Significant heat removal through the steam generators is no longer possible; therefore, the borated water from the HPI system continues to cool the core, and the flow from the small break will be a mixture of steam and water. After two to five hours, the core will have been cooled enough such that bulk boiling stops, and flow from the break transitions to a pure liquid phase.

Within an hour after bulk boiling stops, internal heat movement occurs via the liquid, the coolant at the exit of the core begins to return to a subcooled state, and the RCS starts to refill slowly with coolant. Borated water starts to pass backwards over the RCPs and fill the pump suction pipe. The slug of deboreted water that had accumulated in the pump suction pipe and the lower plenum of the steam generator is then pushed back into the upper plenum of the steam generator. After another one to two hours, the coolant at the core exit becomes more subcooled, and the operator will open the high point vents, allowing the system to refill more quickly. After another one to two hours, the system fills to the hot leg spill over part of the core, and natural circulation begins.

Once natural circulation begins, the slug of deboreted water in the steam generator is pushed through the pump suction pipe, discharge pipe, downcomer, and then into the lower inlet plenum. This slug of deboreted water flowing through the core leads to a boron dilution event where re-criticality of the core could occur. The entire sequence of events between the beginning of the SBLOCA and the restart of natural circulation may take between six and eleven hours, depending on the location and size of the break.

## 2.6 Boron Dilution Following Restart of Natural Circulation

The earlier SBLOCA analysis [1] for the CR-3 plant was for a  $0.007 \text{ ft}^2$  ( $6.5 \text{ cm}^2$ ) break with no operator intervention and yielded a boron dilution event following the restart of natural circulation that is characterized by the 500-second curves shown in Figure 2.7. The  $0.007 \text{ ft}^2$  break was considered to be a more conservative case to study because it yielded the highest volume of deboreted water in the steam generator. The volume of deborate that accumulated in the steam generator for this SBLOCA was approximately  $1000 \text{ ft}^3$  ( $29 \text{ m}^3$ ). When natural circulation resumed, the deboreted water was mixed with the highly borated water in the pump suction and discharge pipes. Further mixing of deboreted and borated water occurred in the downcomer of the reactor vessel before entry into the lower inlet plenum.

## 2.7 Transient Analysis of Boron Dilution Events

In the prior analysis for the B&WOG, a one-hour transient simulation of the entire reactor system was performed with RELAP5 to bring the core to conditions that would approximate those at the restart of natural circulation following a  $0.007 \text{ ft}^2$  SBLOCA. This initialization transient imposed boundary conditions for coolant flow at the vessel inlet nozzles, and pressure

at the vessel exit nozzles. After 3400 s, the vessel conditions in the model had evolved to those approximating the restart of natural circulation, as shown in Table 2.4. A coupled neutronic/thermal-hydraulic model of the transient behavior of the CR-3 core during the boron dilution event shown in Figure 2.7 was then performed using RELAP5 with a point-kinetic model used in conjunction with the core inlet boron dilution curve. At 3600 s, the reactivity was forced to zero, and the boron dilution transient was initiated. This point in time corresponds to 160 s in Figure 2.7, when the core inlet boron concentration reaches the critical boron concentration for the CR-3 core (1494 ppm).

**Figure 2.7 Boron Dilution Curves for B&W PWR.**

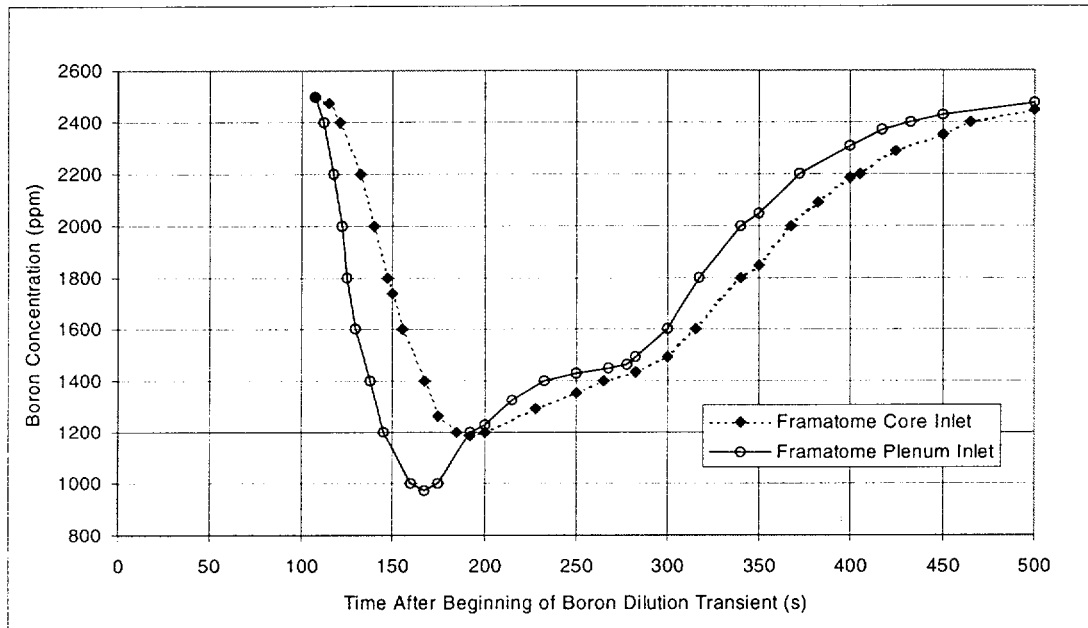


**Table 2.4 Conditions of B&W PWR Cores Before Dilution Transients**

B&W PWR Core	CR-3	TMI-1
Full Power Level	2568 MWth	2772 MWth
Cycle	BOC - Cycle 11	BOC
Reference Power Level	< 1.0e-4 %	< 1.0e-4%
Bank Positions	All Rods In	All Rods In
Xenon Distribution	No Xenon	Equilibrium Xenon
Delayed Neutron Fraction	0.0065	0.006323
Coolant Pressure	6.895 MPa (1000 psia)	15 MPa (2175 psia)
Coolant Temperature	422 K (300°F)	500 K (441°F)
Coolant Flow	3% of Nominal	3% of Nominal
Boron Concentration at Lower Inlet Plenum	2500 ppm	2000 ppm (Case 1) 1339 ppm (Case 2)
Critical Boron Concentration	1494 ppm	1165 ppm
Boron Reactivity Coefficient	-7.575 pcm/ppm	-6.83 pcm/ppm

Using data from the B&WOG analysis of the CR-3 boron dilution events, the similar transient was simulated for TMI-1 at BOC with the three-dimensional coupled PARCS/RELAP5 code. The initial steady-state conditions of the TMI-1 core before the SBLOCA are shown in Table 2.5. The TMI-1 core is at HZP (1.0E-4 % of full power) with the nominal coolant pressure, temperature, and flow rates. The PARCS/RELAP5 code is first used to compute the initial steady-state neutron flux, power, and temperature distributions and the effective multiplication factor at HZP. The computed multiplication factor is used to normalize the neutron source distribution such that the initial reactivity (before SBLOCA) will be zero.

**Table 2.5 Initial Steady-State Conditions for PARCS/RELAP5 Model of TMI-1**

Thermal Power Level (W)	2772
Thermal Power Level (%)	1.0e-4
Boron Concentration (ppm)	1700
Position for Banks 1 to 4	Withdrawn (971 steps)
Position for Banks 5,6,7	Inserted (0 steps)
Position for Bank 8 (APSR)	Partial (300 steps)
Lower Inlet Plenum Coolant Pressure (MPa)	15.085
Lower Inlet Plenum Coolant Temperature (°C)	278
Lower Inlet Plenum Coolant Flow Rate (kg/s)	17, 374
K-Effective	1.00196

Two different boron dilution transients in the TMI-1 core were simulated using PARCS/RELAP5. In the first case (Case 1), the B&WOG curve for the lower inlet plenum (shown in Figure 2.7) was used directly as a time-dependent boundary condition. In the second case (Case 2), the lower inlet plenum boron dilution curve was adjusted such that the time-dependent worth of the boron deficit in the TMI-1 core would be the same as that for the CR-3 analysis. The boron deficit is the dollar worth of the boron reactivity relative to the critical value. For example, at 168 s in Figure 2.7, the boron concentration in the lower inlet plenum is approximately 969 ppm, which is 525 ppm (\$6.12) below the critical value (1494 ppm) in the CR-3 core upon restart of natural circulation. To get the same dollar worth for the boron deficit in the TMI-1 core, the boron concentration at the lower inlet plenum must be approximately 598 ppm, instead of 969 ppm. These calculations are based on the thermal-hydraulic and neutronics properties of both the CR-3 and TMI-1 cores before restart of natural circulation, as shown in Table 2.4.

Following an SBLOCA and before the restart of natural circulation, the coolant pressure, temperature, and flow rates are expected to fall to approximately 6.6 MPa, 150 °C, and 3% of nominal respectively. These are the conditions that should be modeled in the PARCS/RELAP5 simulation of the boron dilution event. Unfortunately, the tabulated two-group cross section data that is used in the PARCS model of the TMI-1 core at BOC were generated for coolant temperatures ranging from 247 to 332 °C (520 to 605 K), and for boron concentrations ranging from 5 to 2000 ppm. Extrapolating the cross section data to very low temperatures introduces uncertainties. Preliminary comparisons with benchmark calculations by colleagues at the RRC-KI [12] have shown discrepancies in the results for the boron dilution event that suggest problems with extrapolating the tabulated data to very low temperatures. As a compromise, the coolant temperature for the restart of natural circulation was changed to 227 °C (500 K), and the boron concentration was not allowed to go above 2000 ppm. However, as shown in Table 2.6, raising the coolant temperature to 500 K would significantly reduce the subcooling, and this could seriously affect the coupled neutronic/thermal-hydraulics behavior. To get approximately the

same subcooling at 500 K as at 6.6 MPa and 422 K, the pressure was not reduced to 6.6 MPa during the transient, but maintained at 15 MPa. As shown in Table 2.6, water at 15 MPa, 500 K has approximately the same subcooling as water at 6.6 MPa, 422 K.

The critical boron concentration in the PARCS simulation of the TMI-1 core was found with a long transient simulation where the reactivity approached zero after the reactor was scrammed and the coolant pressure, temperature, and flow rate were adjusted to the values desired before the beginning of the boron dilution transient. By trial and error, the critical boron concentration in the TMI-1 core was found to be approximately 1165 ppm, which is about 329 ppm lower than that in the CR-3 core.

To bring the TMI-1 core from the initial HZP steady state conditions to the conditions after the SBLOCA and before the restart of natural circulation and the boron dilution events (see Table 2.4), an artificial 100-second initialization transient was performed with PARCS/RELAP5, linearly adjusting the control rod positions, coolant flow rate, temperature, and boron concentration. The pressure was maintained at 15 MPa. The reactor was scrammed in the first 10 s. Most of the initialization transient was used to bring the system to relatively stable thermal-hydraulic conditions before the boron dilution event was begun. In Case 1, the boron concentration was raised to 2000 ppm to bring the TMI-1 core to a highly subcritical state. In Case 2, the boron concentration was lowered to 1165 ppm to bring the reactor to a near-critical state. In fact, this would actually bring the reactor to a slightly super-critical state, but the power level would still remain relatively insignificant (less than 1%) before the boron dilution event began.

The two boron dilution events simulated with the PARCS/RELAP5 model are shown in Figure 2.8. Both simulations were run for an additional 200 s following the 500-second boron dilution transient, and the 100-second initialization transient to allow the core to approach a relatively stable thermal-hydraulic state. Hence, the total length of the PARCS-RELAP5 simulation was 800 s. The boron concentration was allowed to exceed 2000 ppm in the latter portion of the dilution event, long after the dominant effects would occur.

**Table 2.6 Flow Conditions Before Restart of Natural Circulation**

Flow Conditions	Original	Contemplated	Modified
Pressure (MPa)	6.6	6.6	15.1
$T_{\text{sat}}$ (K)	555	555	615
$h_f$ (kJ/kg)	1244	1244	1612
$h_{fg}$ (kJ/kg)	1533	1533	1003
$T_{\text{inlet}}$ (K)	422	500	500
$h$ (kJ/kg)	631	976	978
$\Delta h_{\text{subcooled}}$ (kJ/kg)	613	268	634
Subcooling Change (%)	N/A	-56	+3.4

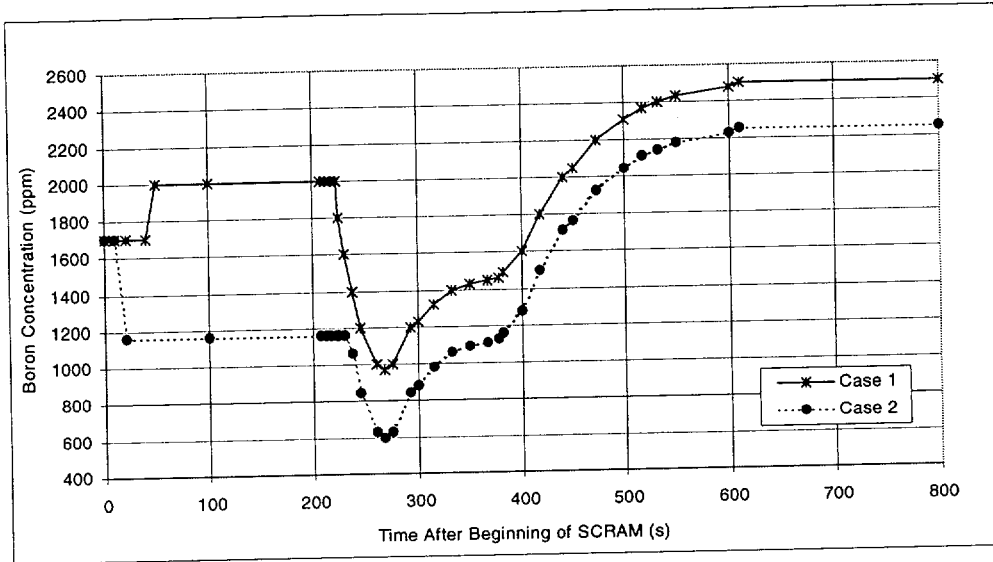


**Figure 2.8 Boron Dilution Curves for TMI-1 Analysis**

### 3. DISCUSSION OF RESULTS

#### 3.1 Transient Analysis with Boron Dilution - Case 1

In the Case 1 boron dilution event shown in Figure 2.8, the boron concentration drops from 2000 ppm at 207 s to the near-critical value of 1165 ppm at 247 s. After the minimum of 969 ppm occurs at 267 s, the inlet plenum boron goes above 1165 ppm at 290 s, and up to 2500 ppm by 610 s.

The power variation with time is shown in Figures 3.1.1 and 3.1.2 using linear and logarithmic scales respectively. The power increases by several orders of magnitude within 4 s to a maximum value of ~80% at ~273 s. After the initial pulse, the power drops down to ~10% at 275 s, then drops below 10% at 282 s, and then drops below 1% after 298 s. The full width half maximum (FWHM) of the first power pulse is approximately 94 ms.

The total reactivity is shown in Figures 3.1.3 and 3.1.4. Boron dilution causes the TMI-1 core to go critical at ~269 s, and prompt critical at ~273 s, a difference of less than 4 s. The reactivity peaks at ~\$1.02 at 273 s, just preceding the peak power. A number of fluctuations in the reactivity occur afterwards due to changing boron concentration and competing feedback mechanisms from the fuel and moderator, with another peak occurring at 281 s (\$0.25). After 285 s, the total reactivity drops below zero and remains negative for the remainder of the transient.

Plots of the maximum fuel pellet temperature and enthalpy are shown in Figures 3.1.5 and 3.1.6. The hottest fuel pellet is usually found in FA-151/TH-27 at 37 cm above the bottom of the core. The hottest fuel pellet jumps from 227 °C (14 cal/g) at 272 s to 480 °C (30 cal/g) at 275 s. Cooling by the moderator causes the fuel pellet temperature to drop gradually to 284 °C (17 cal/g) by 300 s, and then back to 227 °C by 400 s.

Since it is difficult to accurately define isolated reactivity components in a consistent way, one must treat the calculation of the reactivity components with caution. Many algorithms fail to match the sum of the individual components with the total reactivity exactly and require an adjustment of components loosely based on physical insight. The PARCS procedure attempts to avoid this by calculating the cumulative effect of each component on the reactivity, and taking the difference in the cumulative reactivity as the component reactivity. Of course, this procedure is highly dependent on the sequence for the evaluation of the reactivity components, and one must still regard the evaluation of the reactivity components with some caution.

Plots of the various reactivity components are shown in Figures 3.1.7 and 3.1.8. Since the fuel and moderator temperatures and densities are relatively unchanged at the end of the transient in comparison to the beginning, it is expected that the reactivity components should be unchanged as well. The shape of the boron reactivity component is similar to the total reactivity. This is not surprising since the boron dilution process dominates the reactivity effect on the transient. The changes in the reactivity components at the end of the transient in comparison to the beginning can be attributed to the changes in the flux distributions and the concentrations of delayed neutron precursors.

Plots of the core average and minimum boron concentration are shown in Figures 3.1.9. The core average boron concentration goes below 1165 ppm, the critical value, at 276 s, reaches a minimum value of 1108 ppm at 281 s, and then goes above 1165 ppm at 298 s. The minimum

boron concentration drops to 1008 at 277 s in TH-27 in axial plane k=5 ( $z \sim 7$  cm), near the bottom of the core. There isn't sufficient localized heat generation at the given pressure to cause void formation in any part of the core..

Because there is a simultaneous spatial and transient variation of the boron concentration in the core, the reactivity response of the reactor will be different from that which would be predicted by a point-kinetics model using either the core inlet or core-average boron concentration. For example, the lower inlet plenum boron concentration drops to the critical value at 247 s, while the core average boron concentration reaches 1165 ppm at 276 s. However, the core goes critical at 269 s. The slug of water in the bottom of the core becomes diluted enough to cause the reactor to go critical before the core average boron concentration drops below 1165 ppm. Hence, one can see the value in using a 3-D, time-dependent coupled neutronics/thermal-hydraulics model to get a more accurate representation of the effect of boron dilution on core criticality.

Axial power distributions are shown in Figures 3.1.10 and 3.1.11 for the average plane, and for the hot channel (FA-151, TH-27). The planar average power is peaked towards the bottom of the core, but as the fuel and coolant heat up, this peak becomes flattened. The planar averaged peak drops from approximately 3.2 to 2.7 between the time of the peak power at 273 s, and the time of the peak fuel pellet enthalpy at 275 s. The relative power for the hot channel peaks at 2.6 in axial plane 5 ( $z=37.2$  cm) at 273 s, but as the fuel and coolant heat up due to energy deposition and heat transfer, the power distribution becomes more flattened. The power is more peaked at the bottom due to the lower boron concentration. In addition, there is a short length (14.4 cm) of the core at the bottom that has no insertion of control rods. The assembly-averaged radial power distribution is shown in Figure 3.1.12, and the radial power distribution in axial plane k=5 ( $z=37.2$  cm) is shown in Figure 3.1.13. Both distributions are at  $\sim 275$  s. Clearly, the relative power is highest in the hot channel (TH-27). The second-highest power assembly is TH-23.

Axial boron concentration distributions are shown for the planar average and the hot fuel channel in Figures 3.1.14 and 3.1.15 for time intervals ranging from 273 to 277 s. These plots well illustrate the progression of the diluted slug of water through the core. Initially, the axial boron concentration distribution in the hot channel (TH-27) is approximately the same as the planar average, but after the power peaks at 273 s, the coolant starts to heat up more quickly in the hot channel and the diluted water at the lower inlet plenum flows preferentially into the hot channel, giving it a more diluted axial distribution within a matter of a few seconds. The low boron concentration at the inlet augments axial power peaking near the bottom of the core. The assembly-averaged boron concentration radial distribution is shown in Figure 3.1.16, and the radial distribution of boron concentration in axial plane 5 ( $z \sim 37$  cm) is shown in Figure 3.1.17. Both distributions are at  $\sim 277$  s. The boron concentration is lowest in the hot channel (TH-27), and this is more noticeable with the assembly-averaged values.

The low boron concentration in TH-27 is consistent with the high relative power, and this suggests an auto-catalytic effect where diluted water from the inlet plenum flows preferentially through the hot channel due to reduced thermal-hydraulic resistance and larger buoyancy forces. The hot channel has a low burnup and no control rods present; thus the neutron flux and power deposition is higher. Higher heat transfer raises the coolant temperature and lowers the density and viscosity. The difference in coolant density between the hot channel and the outer channels and the bypass (TH-30), as illustrated by the sample assembly-averaged radial coolant density distribution at  $\sim 277$  s in Figure 3.1.18, drives natural circulation. Highly diluted water from the lower inlet plenum mixes with the bypass flow and return flows from other channels, and then is pushed preferentially into the hot channel. As more diluted water flows through the hot channel,

the neutron flux and power deposition within the hot fuel assembly will increase due to reduced neutron absorption in the moderator. This autocatalytic effect reverses after the boron concentration at the lower inlet plenum increases, although the reversal is delayed due to the return flow of diluted water from the bypass and other channels.

The effect of natural circulation is further illustrated by the normalized mass flux radial distributions at the inlet and exit of the core at ~277 s shown in Figures 3.1.19 and 3.1.20. There is a strong correspondence between the radial power, coolant density and mass flux distributions. Channels with the lowest coolant densities (TH-17, 23, 27) have the highest upward mass flow rates due to buoyancy forces. Conversely, channels with the highest coolant densities tend to have the highest downward mass flow rates. Channels that have a relative power above 0.7 tend to have upward flow, while channels with a relative power below 0.3 tend to have downward flow. As shown in the time plots of mass flow rate for channels TH-01, 07, 09, 20, and 25 in Figures 3.1.21 and 3.1.22, flow reversal actually occurs. It is in these channels that the relative power ranges between 0.3 and 0.7. By the end of the boron dilution transient, flow in all channels is upward, including the bypass because the power level drops down to negligible levels, and radial density variations that would cause natural circulation disappear.

The probability of departure from nucleate boiling for an average fuel rod within an assembly is extremely low during this boron dilution event since the DNBR does not go below 5, and there is no void formation. However, it may be necessary to consider performing a more detailed sub-channel thermal-hydraulic analysis to account for flow and power variations within a fuel assembly, particularly in the hot channel and the low-flow, low coolant density channels.

There are several reasons why the location of the highest change in fuel pellet enthalpy (the "hot spot") occurs in FA-151/TH-27. First, FA-151 is a low-burnup fuel assembly, and so it will have a higher fission rate. Second, FA-151 has no control rod assembly in it to absorb neutrons and reduce the local flux. Third, FA-151 has only two adjacent fuel assemblies with control rods inserted. Other low-burnup, un-rodded assemblies that might be expected to have higher flux and power depositions are surrounded by 4 assemblies with control rods inserted. Although FA-110 / TH-14 has a low burn-up, it is still surrounded by 3 rodded fuel assemblies.

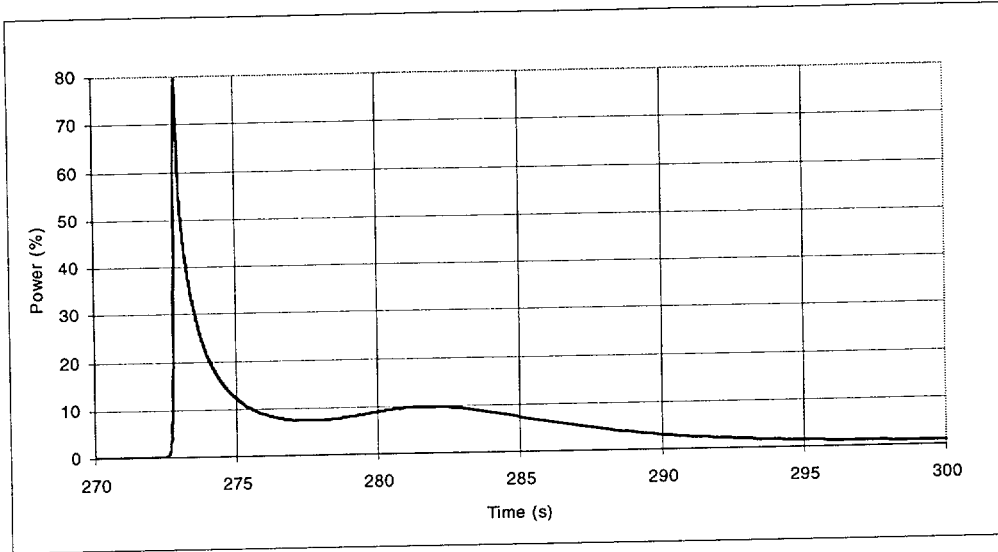


**Figure 3.1.1 Power Variation in Case 1**

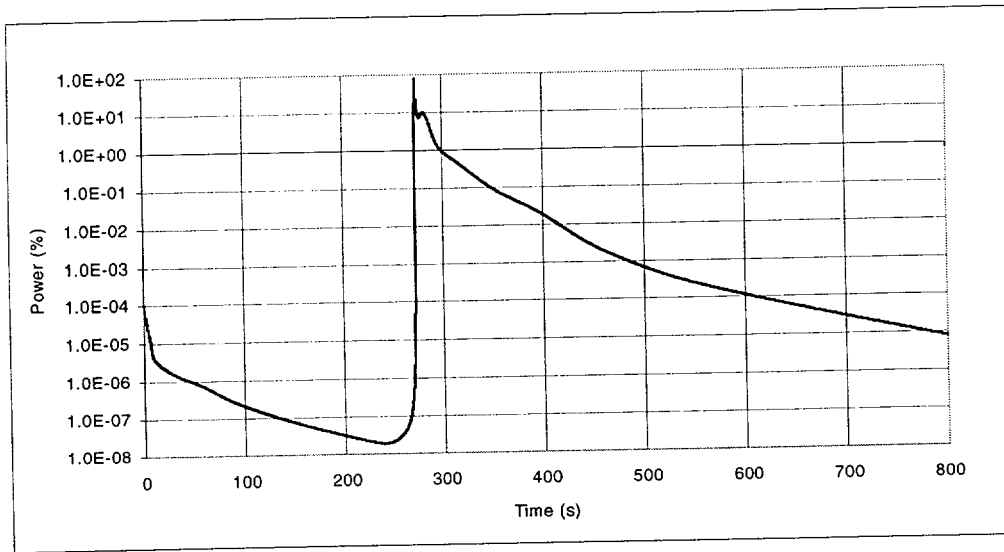


**Figure 3.1.2 Logarithmic Power Variation in Case 1**

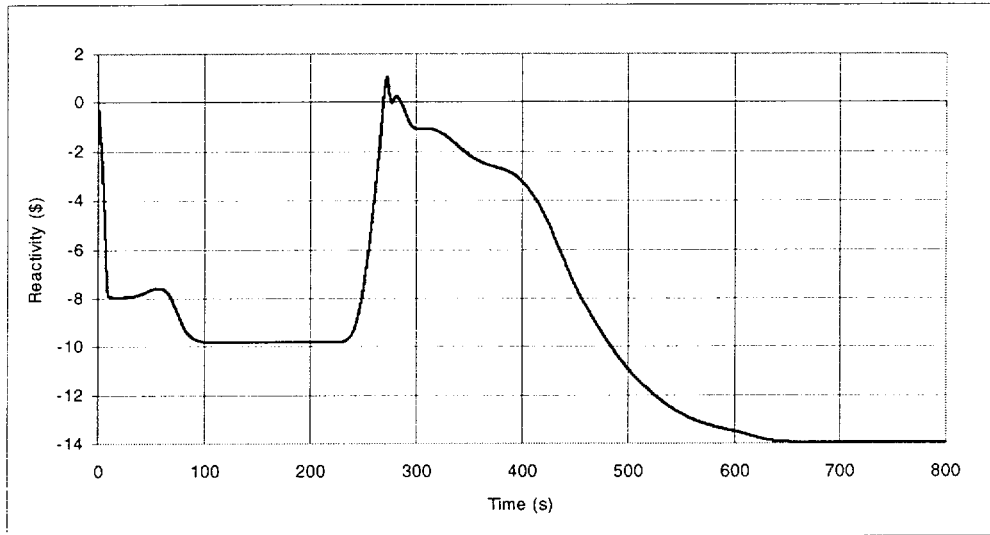


**Figure 3.1.3 Total Reactivity Variation in Case 1**

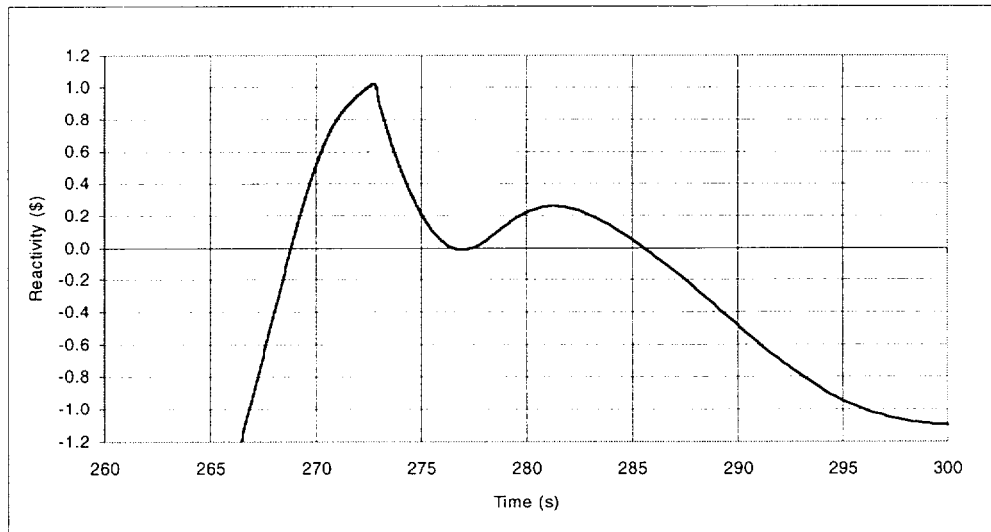


**Figure 3.1.4 Reactivity in Case 1 from 260 to 300 s**

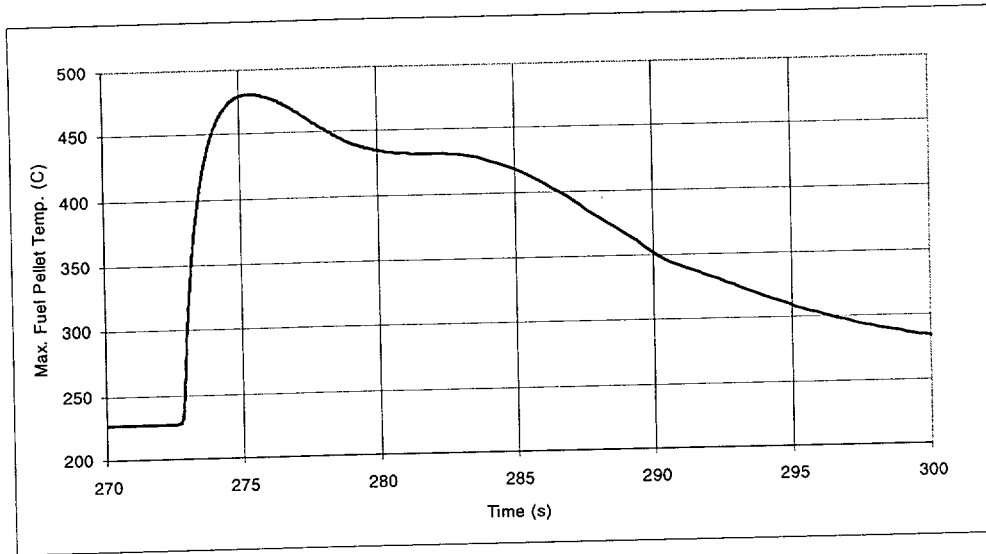


**Figure 3.1.5 Maximum Fuel Pellet Temperature in Case 1**

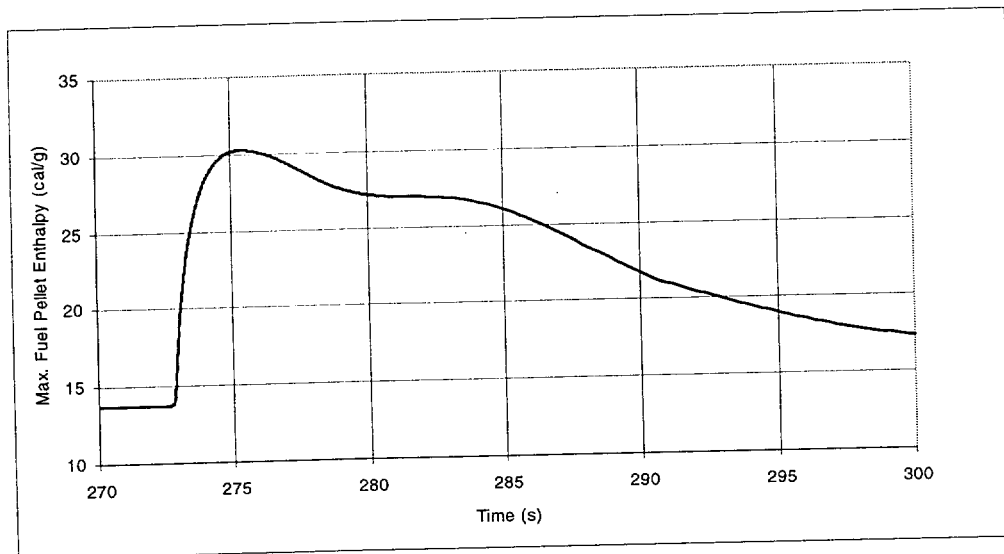


**Figure 3.1.6 Maximum Fuel Pellet Enthalpy in Case 1**

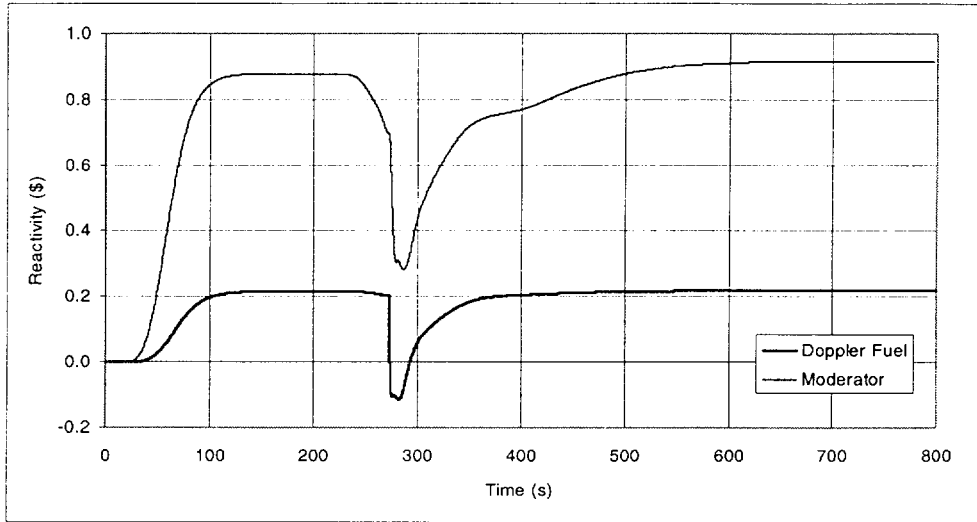


**Figure 3.1.7 Doppler and Moderator Reactivities in Case 1**

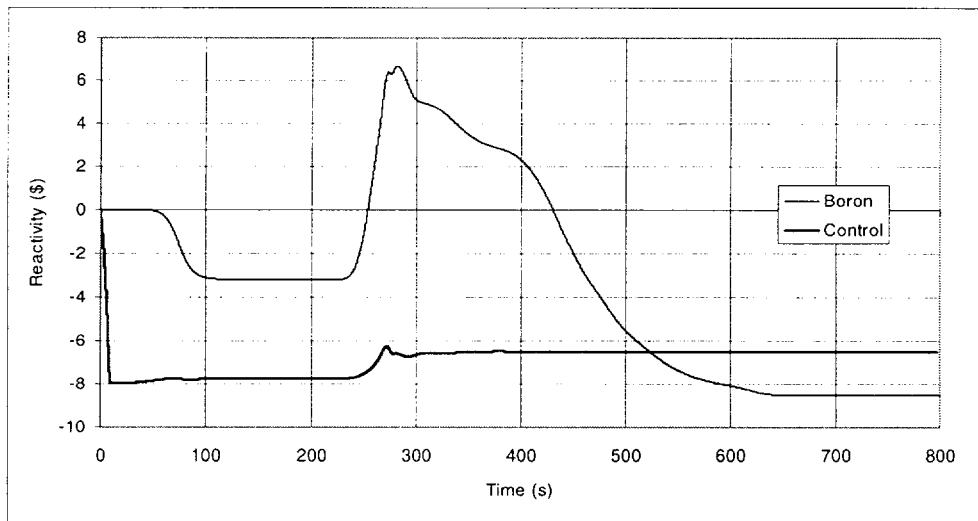


**Figure 3.1.8 Boron and Control Reactivities in Case 1**

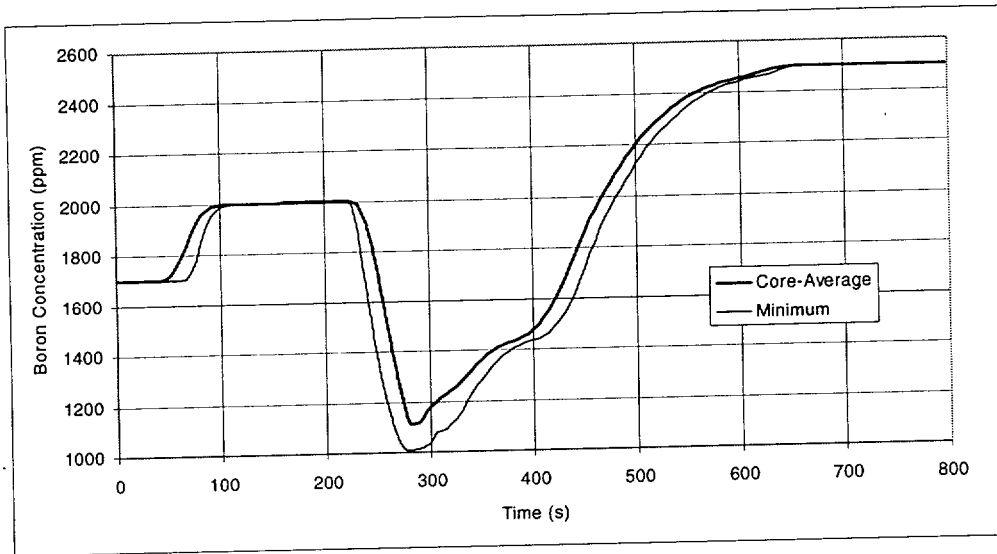


**Figure 3.1.9 Core Average and Minimum Boron Concentration in Case 1**

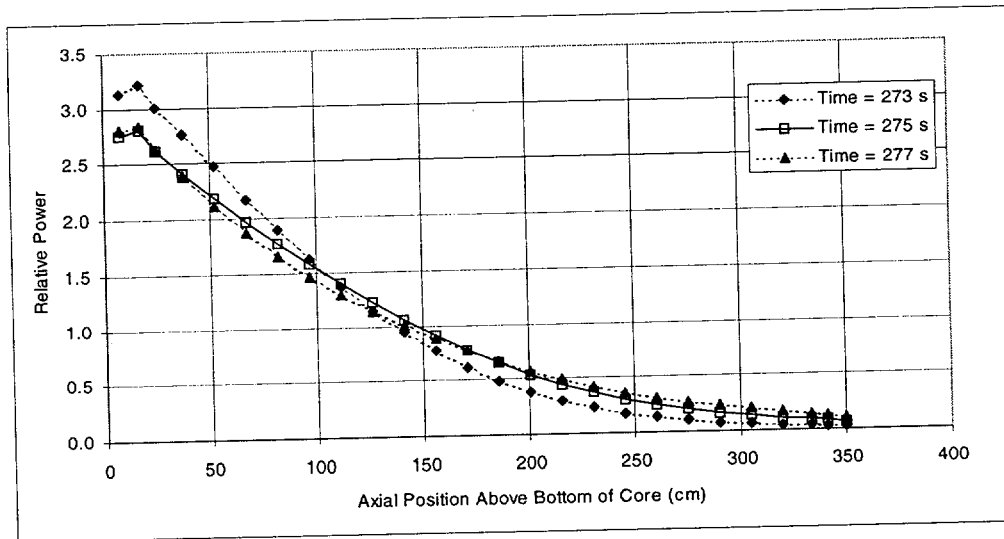


**Figure 3.1.10 Axial Power Distribution in Case 1**

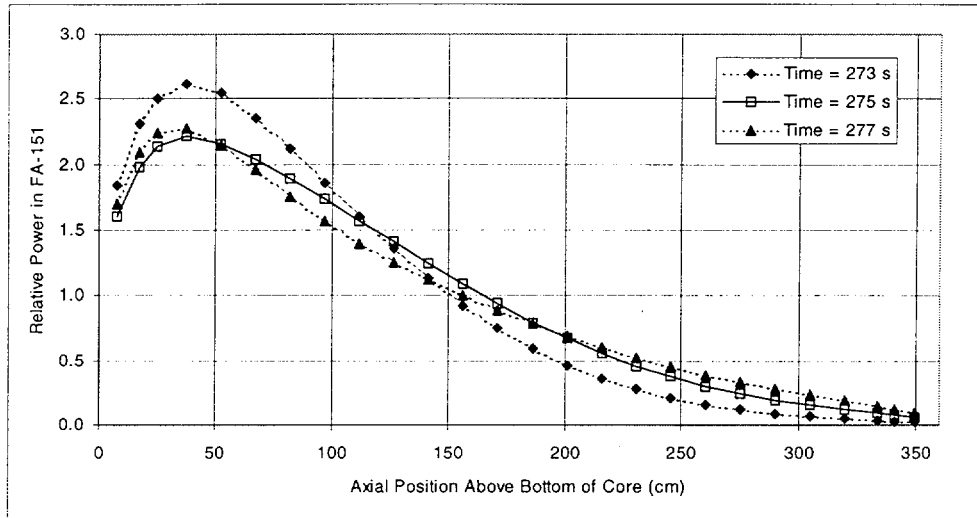


Figure 3.1.11 Axial Power Distribution in FA-151 (TH-27) in Case 1

0.509	0.905	0.711	1.153	0.796	1.018	0.437	0.204
	0.637	1.091	0.854	1.362	0.786	0.850	0.251
		0.854	1.533	1.506	1.308	0.497	0.185
			1.166	1.896	1.001	0.686	
				1.481	<b>2.230</b>	0.722	
					1.246		

Figure 3.1.12 Assembly-Averaged Radial Power Distribution at Time ~ 275 s in Case 1

0.562	1.012	0.767	1.234	0.826	1.058	0.446	0.217
	0.695	1.183	0.892	1.419	0.798	0.881	0.265
		0.894	1.579	1.595	1.293	0.454	0.186
			1.147	1.831	0.932	0.649	
				1.351	<b>2.043</b>	0.668	
					1.131		

Figure 3.1.13 Radial Power Distribution in Axial Plane k=5 (z=37 cm) at Time ~ 275 s in Case 1

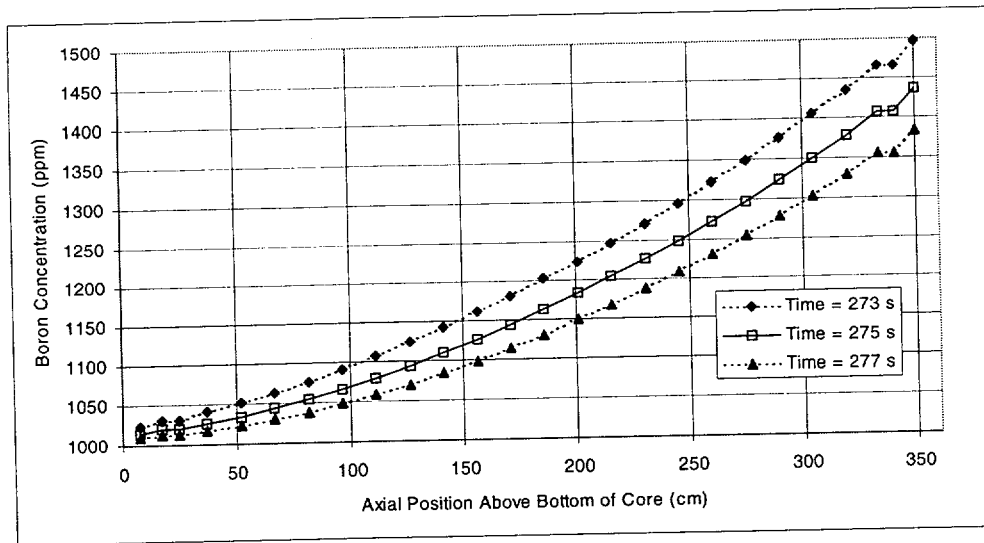


Figure 3.1.14 Plane-Average Axial Boron Distribution in Case 1

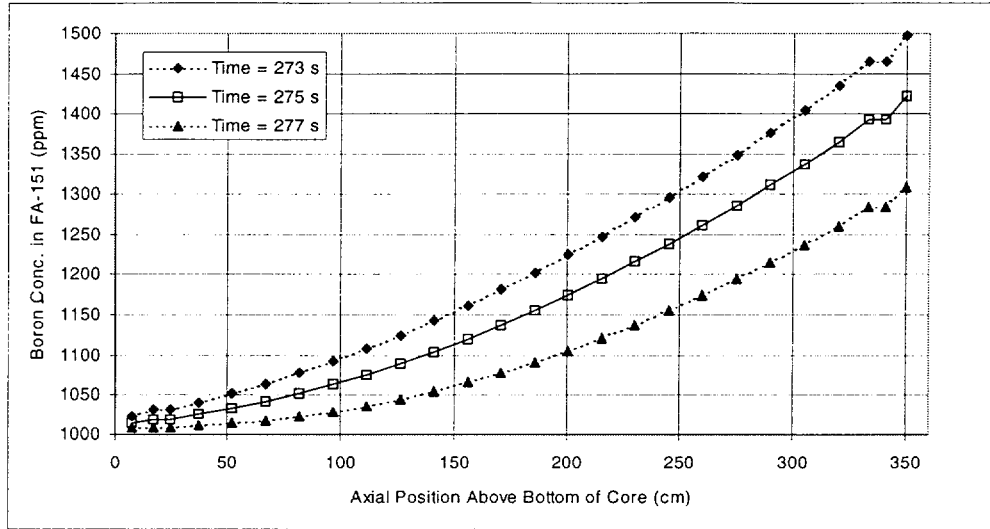


Figure 3.1.15 Axial Boron Distribution in FA-151 (TH-27) in Case 1

1166	1153	1159	1144	1156	1149	1169	1176
	1161	1146	1154	1138	1157	1155	1175
		1154	<b>1132</b>	1133	1139	1166	1177
			1144	<b>1121</b>	1149	1160	
				1134	<b>1111</b>	1159	
					1141		

Figure 3.1.16 Assembly-Averaged Radial Boron Distribution at Time ~ 277 s in Case 1

1022	1018	1020	1016	1019	1017	1022	1025
	1020	1017	1019	1015	1019	1019	1024
		1019	<b>1014</b>	1014	1015	1022	1025
			1016	<b>1012</b>	1017	1020	
				1014	<b>1011</b>	1020	
					1016		

Figure 3.1.17 Radial Boron Distribution at Plane k=5 (z=37 cm) at Time ~ 277 s in Case 1

835	828	832	823	830	826	837	840
	833	825	829	819	831	830	840
		829	<b>815</b>	816	820	836	840
			823	<b>807</b>	826	832	
				816	<b>798</b>	832	
					822		

Figure 3.1.18 Assembly-Averaged Radial Coolant Density Distribution at Time ~ 277 s in Case 1

0.239	1.011	0.661	1.475	0.802	1.212	0.085	-0.368
	0.516	1.363	0.945	1.846	0.769	0.877	-0.276
		0.916	<b>2.153</b>	2.077	1.751	0.221	-0.391
			1.510	<b>2.772</b>	1.231	0.578	
				2.068	<b>3.327</b>	0.655	
					1.639		

**Figure 3.1.19 Normalized Mass Flux Distribution in Case 1 at Time ~ 277 s at Inlet Junctions of Core (Mass Flux Average = 104.246 kg/m<sup>2</sup>/s, Total Flow Area = 5 m<sup>2</sup>)**

0.269	0.998	0.665	1.443	0.798	1.190	0.124	-0.299
	0.529	1.335	0.934	1.806	0.768	0.871	-0.213
		0.906	<b>2.109</b>	2.034	1.712	0.251	-0.321
			1.475	<b>2.727</b>	1.207	0.586	
				2.025	<b>3.278</b>	0.658	
					1.601		

**Figure 3.1.20 Normalized Mass Flux Distribution in Case 1 at Time ~ 277 s at Outlet Junctions of Core (Mass Flux Average = 119.87 kg/m<sup>2</sup>/s, Total Flow Area = 5 m<sup>2</sup>)**

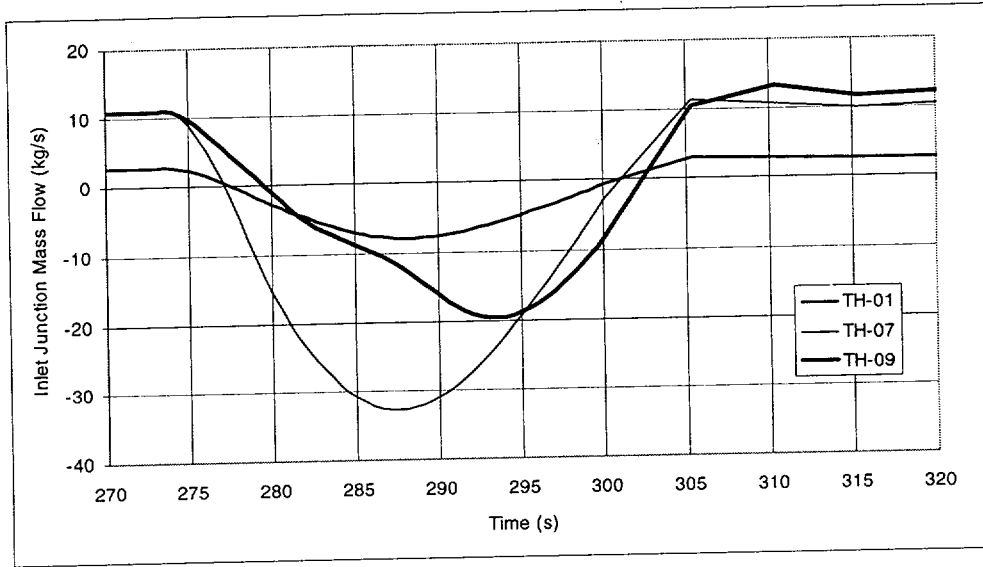


**Figure 3.1.21 Inlet Mass Flow in Channels TH-01, TH-07, and TH-09 in Case 1**

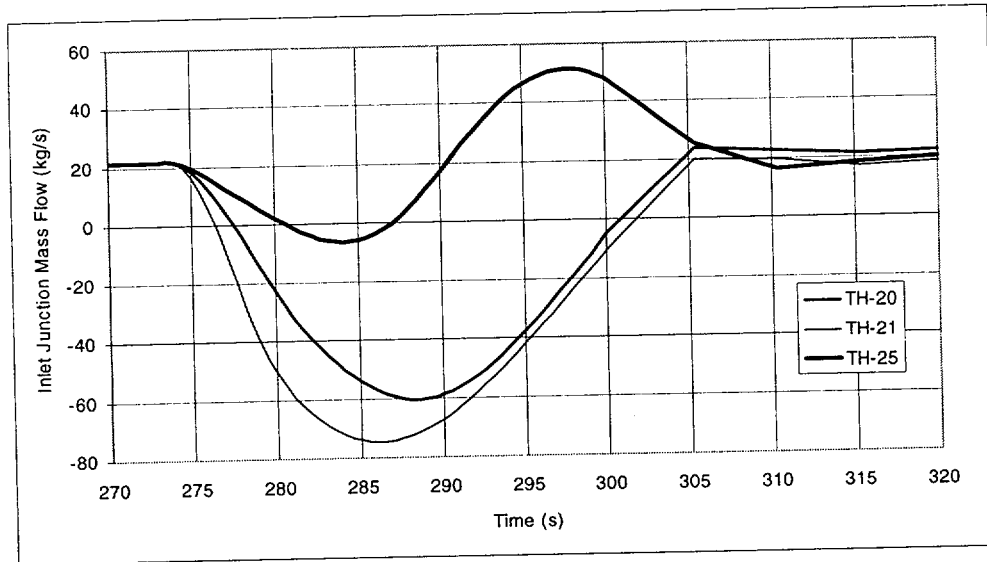


**Figure 3.1.22 Inlet Mass Flow in Channels TH-20, TH-21, and TH-25 in Case 1**

### 3.2 Transient Analysis with Boron Dilution - Case 2

The purpose of using the Case 2 boron dilution curve, as explained in Section 2.7 and shown in Figure 2.8 is to make the analysis more similar to the one done for the B&WOG [1]. The boron reactivity worth relative to the just-critical condition should be approximately the same, and the total reactivity should be approximately zero at the beginning of net boron dilution. Hence, the boron concentration in the lower inlet plenum does not drop below 1165 ppm until 230 s. The minimum of 599 ppm occurs at 267.5 s, and the boron concentration does not go back up to 1165 ppm until 383 s. By the end of the transient (600-800 s), the concentration settles at 2251 ppm.

Power plots using linear and logarithmic scales are shown in Figures 3.2.1 and 3.2.2. The low boron concentration (1165 ppm) and near-zero core reactivity before dilution, along with the more diluted boron curve leads to a few oscillations in the reactivity and power due to competing feedback mechanisms from the Doppler fuel temperature and moderator coolant density. The initial power peak is ~74% at 249 s, followed by smaller peaks of 34% at 255 s, and 16% at 273 s. The power drops below 10% after 290 s, and then below 1% after 400 s as more borated water enters the bottom of core. The width of the first power pulse is approximately 760 ms.

Total reactivity plots are shown in Figures 3.2.3 and 3.2.4. The reactivity before the boron concentration is brought below 1165 ppm is slightly greater than zero, approximately \$0.11, although the power is still negligible ( $\sim 2.0E-4$  %). After further dilution begins at 230 s, the reactivity grows to prompt critical and peaks at \$1.002 at 248.4 s. As it occurs with the power, a period follows when the reactivity undergoes a few oscillations, ranging between \$0.5 and -\$0.2 from 250 to 300 s.

Peak fuel pellet temperature and enthalpy plots are shown in Figures 3.2.5 and 3.2.6. The fuel pellet maximum jumps from 227 °C (13.7 cal/g) at 248 s to 508 °C (32.2 cal/g) at 252 s, and then jumps again to the peak value of 767 °C (50.5 cal/g) at 259 s. The total enthalpy change is approximately 37 cal/g, more than double the value found in Case 1 (16 cal/g). A slight oscillation in the fuel temperature and enthalpy follow due to competing reactivity feedback mechanisms and heat transfer to the coolant. The maximum fuel temperature falls below 500 °C by 300 s, and then below 400 °C by 340 s, and then finally returns to 227 °C by ~520 s. In contrast to Case 1, the peak fuel pellet temperature in Case 2 occurs in FA-137 / TH-23 at 17 cm above the bottom of the core. This location is not the same as that found in Case 1.

Plots of the Doppler fuel and moderator reactivity components are shown in Figure 3.2.7. Due to energy deposition and heat transfer that cause higher fuel temperatures and lower moderator densities, the Doppler fuel and moderator reactivity components decrease in value during the dilution transient. Modest oscillations occur in both components after the initial power pulse, due to competing feedback mechanisms. The Doppler component becomes slightly negative during the transient, going as low as -\$0.6, while the moderator component goes as low as -\$0.9. Oscillations settle and disappear after 320 s, and by the end of the transient, the values of the Doppler and moderator reactivity components are approximately the same as they were before the dilution transient.

Boron and control reactivity components are shown in Figure 3.2.8. Initially, the rapid insertion of the control rods gives a worth of approximately -\$7.9. As the boron concentration is brought up to 1165 ppm and the temperature is reduced to 500 K during the initialization transient, flux distribution changes cause the effective worth to change to -\$6.6. Modest oscillations between -\$6.3 and -\$6.9 occur during the transient, and then the control component settles at -\$6.5. When

the boron concentration is brought down to 1165 ppm before further dilution begins, the boron component is worth \$5.7. At 235 s, the boron component begins to make several jumps, reaching \$6.4 at 250 sec, \$7.6 at 260 s, and \$8.1 at 284 s. As more borated water begins to flow through the core, the boron component drops to zero at 462 s, and settles at -\$5.9 by the end of the simulation. As in Case 1, the total reactivity is largely dominated by the boron dilution. The rate at which the boron (and total) reactivity changes at the beginning of the boron dilution transient is much slower than in Case 1. This occurs because the lower boron concentration in the entire core (1165 ppm) before the dilution transient begins causes the neutron flux distribution to be less bottom-skewed. As mentioned in the previous section, the calculations of the individual reactivity components should be treated with caution due to the difficulty in defining them exactly and accurately.

Plots of the core average and minimum boron concentration are shown in Figures 3.2.9. The core average boron concentration is 1165 ppm before the transient begins, drops down to 1126 ppm at 249 s, reaches a minimum of 812 ppm at 292 s, goes back up to 1165 ppm at 405 s, and then settles at 2251 ppm by end of transient. The minimum boron concentration experiences a few drastic oscillations after the initial power pulse, and in some instances goes as low as 600 ppm. This occurs due to sporadic void formation and collapse. The location of the minimum boron fluctuates, but usually occurs near the bottom of the core in TH-01, 03, 09, 27, and 28.

The time variation of the maximum void fraction in the core is shown in Figure 3.2.10. Void formation tends to be sporadic, with several peaks occurring over a period from 258 to 298 s. The maximum local void fraction goes as high as ~ 41% at 281 s. The highest voids are found in channels TH-01, 09, and 28. The axial location for maximum void fluctuates throughout the core, but the highest voids usually occur near the bottom. Other channels with void formation are shown in Figure 3.2.11. Unlike Case 1, there is sufficient energy deposition and heat transfer to the coolant to cause void formation, and void formation usually occurs in the high-burnup fuel assemblies, with the exception of FA-125/TH-20. In Case 1, there is no void formation.

Normalized axial power distributions for the core and the hot channel (FA-137/TH-23) are shown in Figures 3.2.12 and 3.2.13. The axial power shape becomes much more bottom peaked after dilution begins, as evidenced by the change between 240 and 249 s. The axial distribution becomes most bottom-skewed at 282 s, the time of the lowest minimum boron concentration, and the highest maximum void fraction. The peak planar-average relative power is about 3.9 at 7 cm above the bottom of the core. For the hot channel (the thermal-hydraulic channel with the axial segment of fuel assembly that experiences the highest increase in the fuel pellet enthalpy), the relative power peaks at 4.0 at 17 cm above the bottom of the core. As more borated water begins to flow into the core, the axial power distribution returns to that which existed before the dilution transient. Radial power distributions for assembly-averages and at axial plane k=3 (17 cm above the bottom of the core) at the time of peak fuel temperature (~259 s) are shown in Figures 3.2.14 and 3.2.15. Although the highest normalized assembly-averaged power occurs in TH-23, the highest normalized power at 17 cm is actually in TH-23. The relative power is also quite high in TH-17.

Axial distributions of boron concentration at various time intervals are shown in Figures 3.2.16 and 3.2.17. Here it is seen that at the time of peak power/reactivity, the hot channel distribution is almost the same as the plane average, with the diluted slug near the bottom of the core. As time progresses beyond the initial power pulse, water from the inlet plenum flows preferentially through the hot channel due to natural circulation forces. Thus, the hot channel responds more quickly to changes in the boron concentration in the lower inlet plenum. This explains why the

boron concentration in the hot channel becomes lower than the planar average after 249 s, and then reverses after 292 s. Boron radial distributions for assembly averages and in a specific plane ( $k=3$ ,  $z\sim 17$  cm) at  $\sim 282$  s are shown in Figures 3.2.18 and 3.2.19. The lowest assembly-average boron concentrations are found in TH-27, 23, and 17, which are also the highest power assemblies. The lowest boron concentration at 17 cm above the bottom of the core is found in TH-01, although TH-27, 23, and 17 are quite low as well. The low boron level in TH-01 at 17 cm is due to the high void level at 282 s.

Axial void distributions for FA-89 / TH-01 are shown in Figures 3.2.20 and 3.2.21 at several time intervals. As mentioned previously, void formation and collapse is sporadic, lasting only for a few seconds at most. Void profiles at different time intervals suggest that voids usually form near the bottom of the core, migrate upwards, and then collapse. However, instances of flow reversals or stagnation can occur, permitting substantial latent heat energy deposition in the local coolant and void formation. The speed of the peaks illustrated in the axial void distributions are approximately the same as the time-average speed of the liquid phase of the coolant.

The radial distribution of assembly-averaged coolant density at 282 s is shown in Figure 3.2.22. The coolant density is lowest in channels TH-27, 23, and 17. All are below  $690 \text{ kg/m}^3$ . Coolant densities are highest in TH-08, 15, and 21. A corresponding snapshot of the radial distributions for the normalized mass flux at the inlet and exit of the core at 282 s are shown in Figures 3.2.23 and 3.2.24. There are several noticeable phenomena. Like Case 1, there is a strong correspondence between the radial power, coolant density, and mass flux distributions.

The flow is predominantly upward for any fuel assembly where the relative power is high (greater than 0.7) and the coolant density is low (less than  $700 \text{ kg/m}^3$ ) and vice versa. Exceptions occur in channels TH-01, 25, and 28 where there is flow stagnation and reversal, and this is consistent with the void formation in these channels. This flow reversal is better illustrated in the time plots of channel mass flows in Figures 3.2.25 and 3.2.26. Flow oscillations are occurring in channels TH-01, 07, 09, 20, 25, and 28, and these are driven by natural circulation forces. The highest mass fluxes at both the inlet and exit are found in TH-27, 23, and 17. The lowest mass fluxes at the inlet and exit are in TH-09.

Although the energy deposition is much higher in Case 2, and although there are instances of low flows and void formation, the probability of departure from nucleate boiling remains low since the departure from nuclear boiling ratio (DNBR) ratio for the average fuel pin in an assembly never drops below 3. However, as in Case 1, there are potential uncertainties in the prediction of local thermal-hydraulic conditions and the critical heat flux. Therefore, further analysis of the boron dilution event using a finer resolution of the thermal-hydraulic channels is recommended.

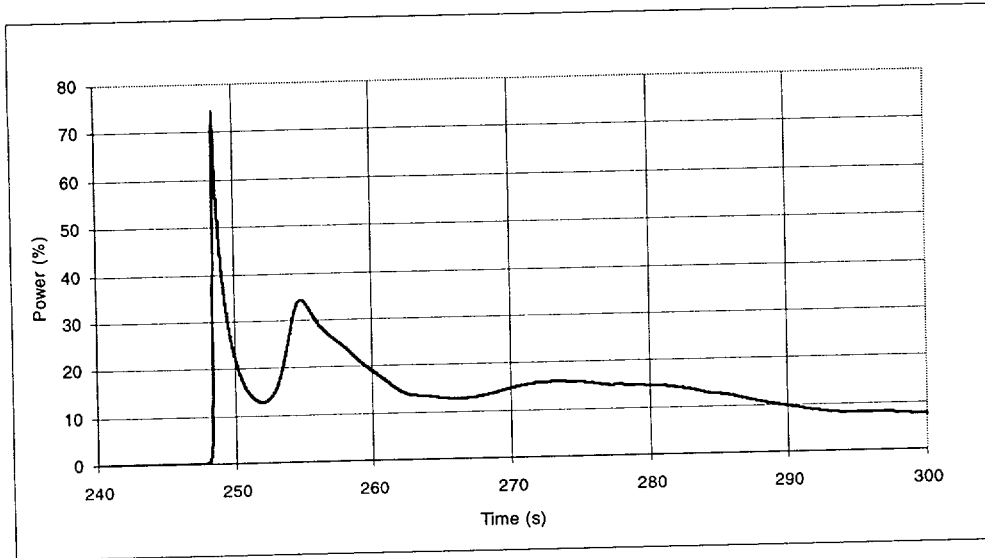


**Figure 3.2.1 Power Variation in Case 2**

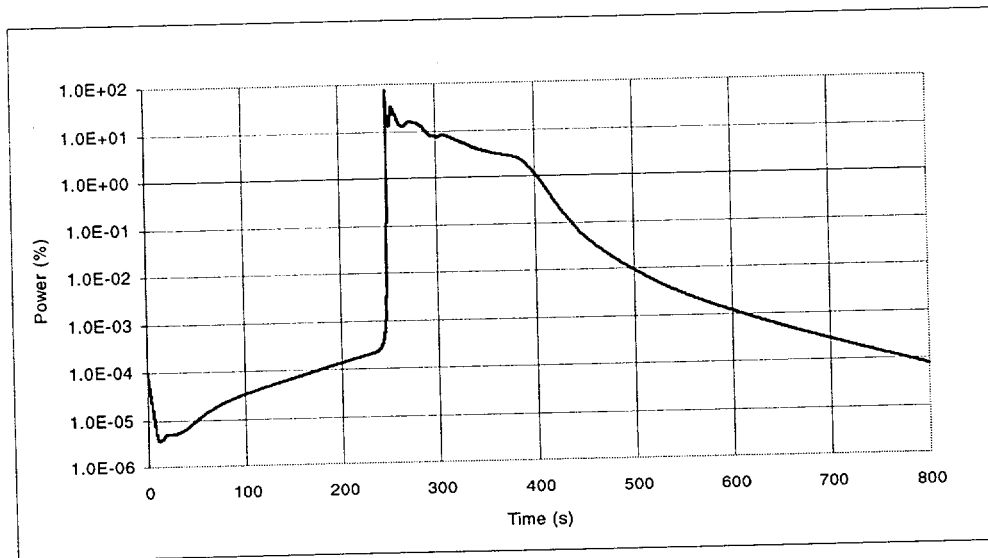


**Figure 3.2.2 Logarithmic Power Variation in Case 2**

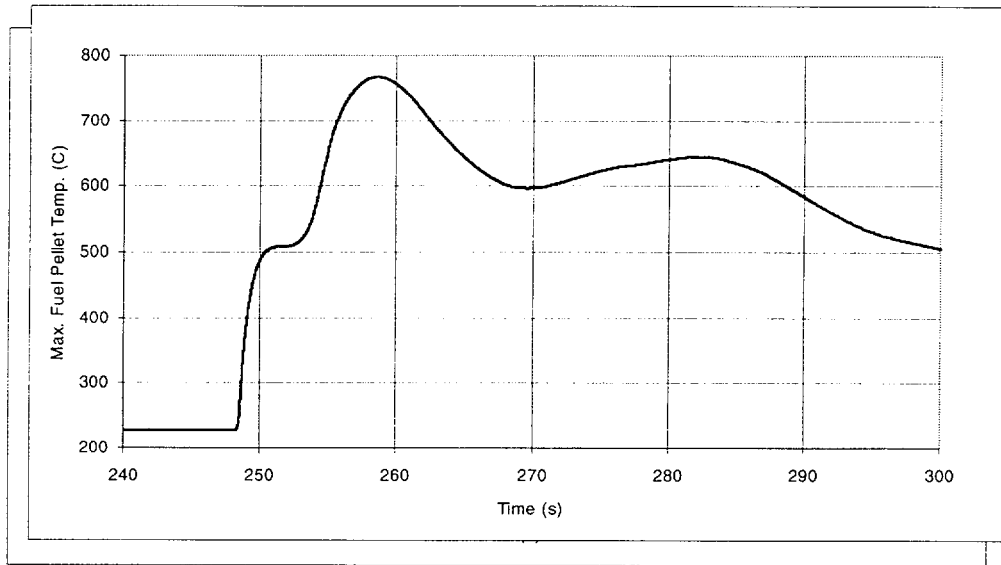


**Figure 3.2.3 Total Reactivity Variation in Case 2**

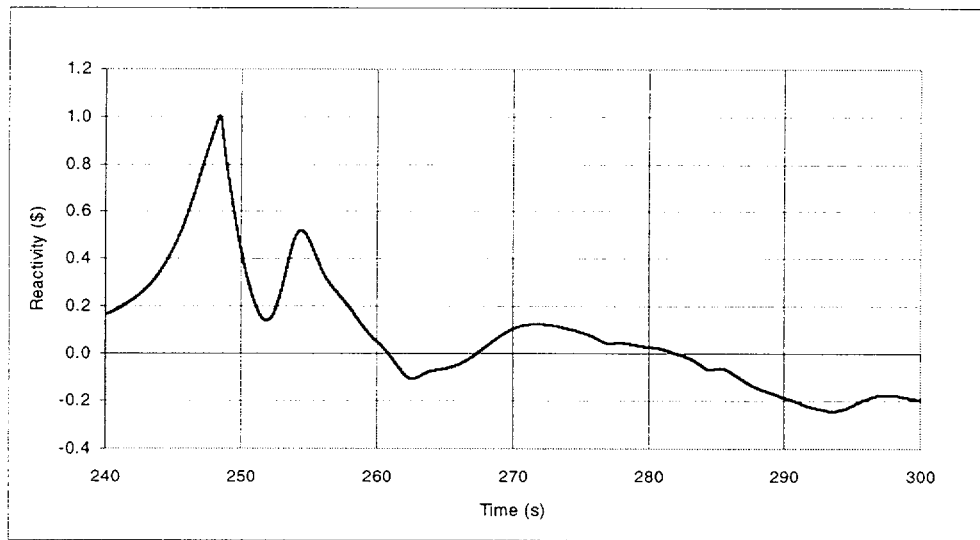


**Figure 3.2.4 Reactivity in Case 2 at 240 to 340 s**

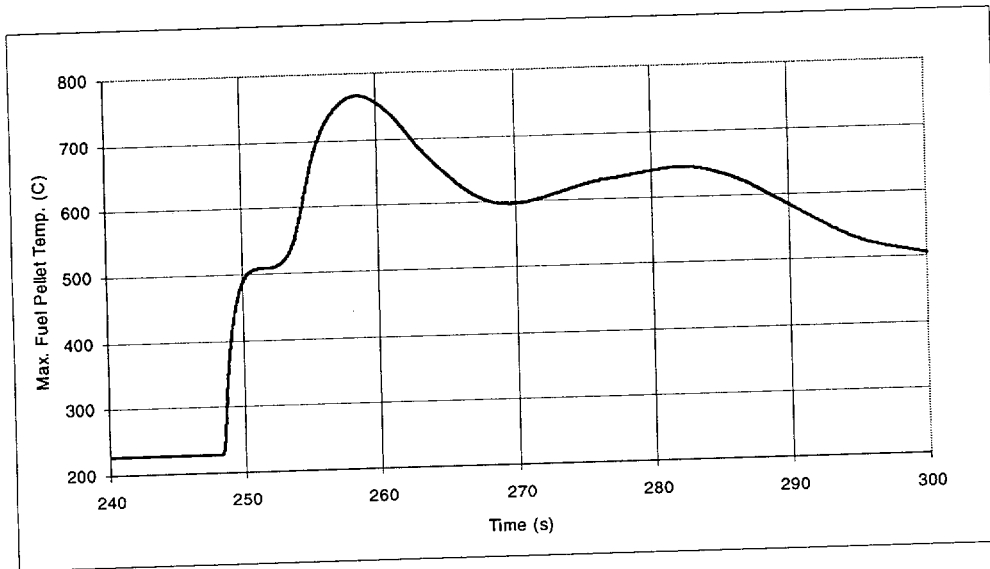


**Figure 3.2.5 Maximum Fuel Pellet Temperature in Case 2**

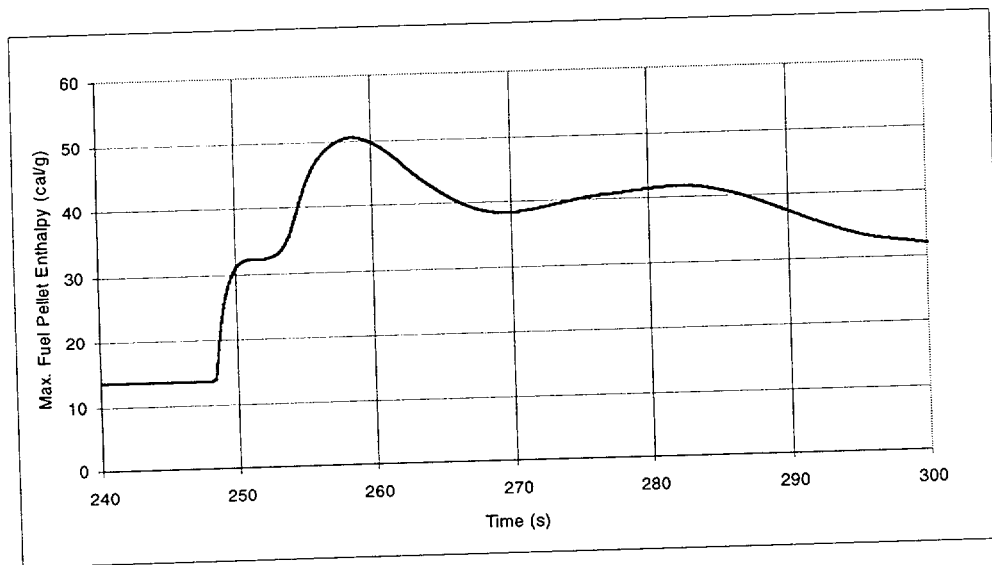


**Figure 3.2.6 Maximum Fuel Pellet Enthalpy in Case 2**

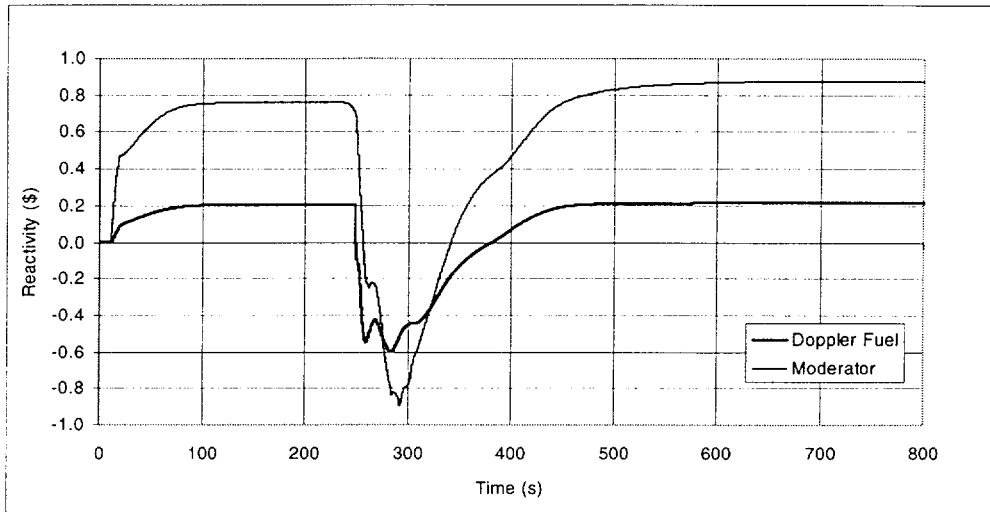


**Figure 3.2.7 Doppler and Moderator Reactivities in Case 2**

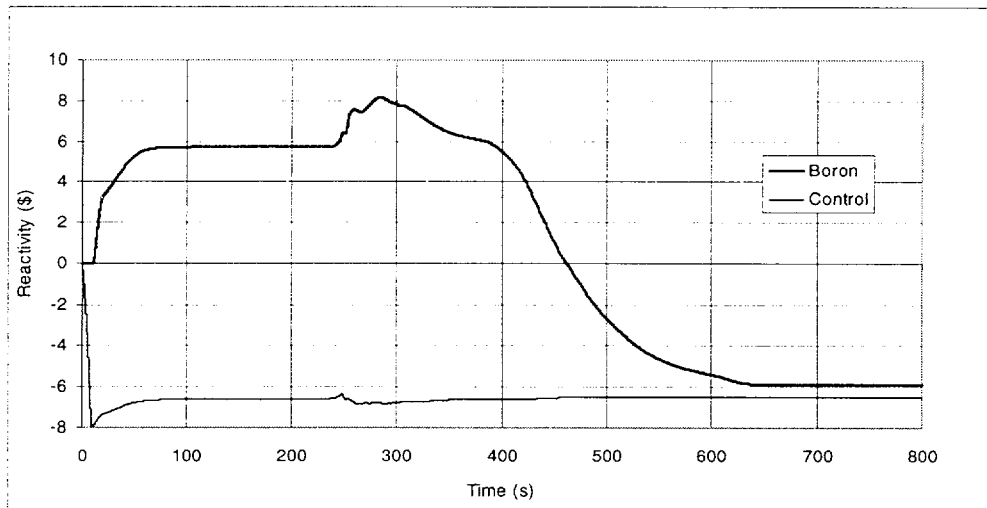


**Figure 3.2.8 Boron and Control Reactivities in Case 2**

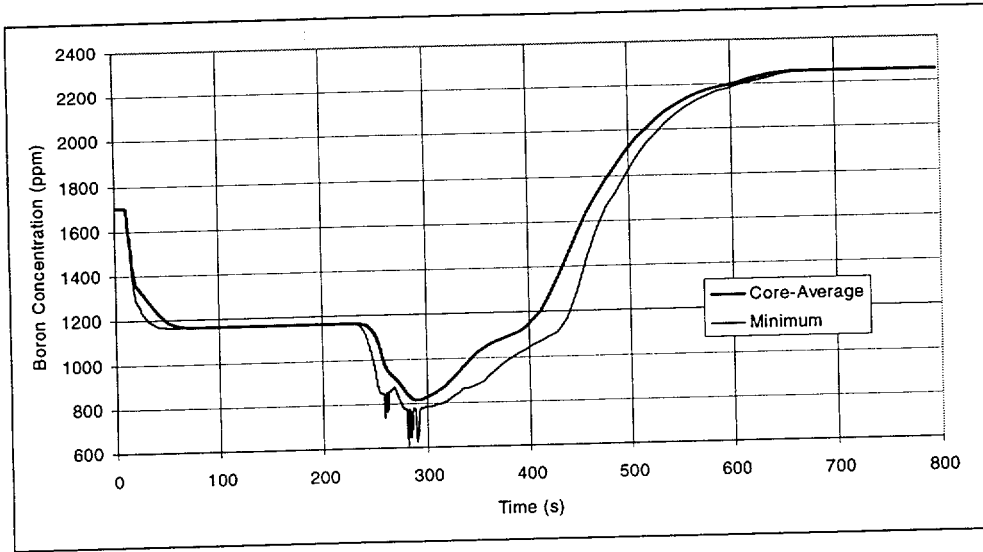


**Figure 3.2.9 Core-Average and Minimum Boron Concentration in Case 2**

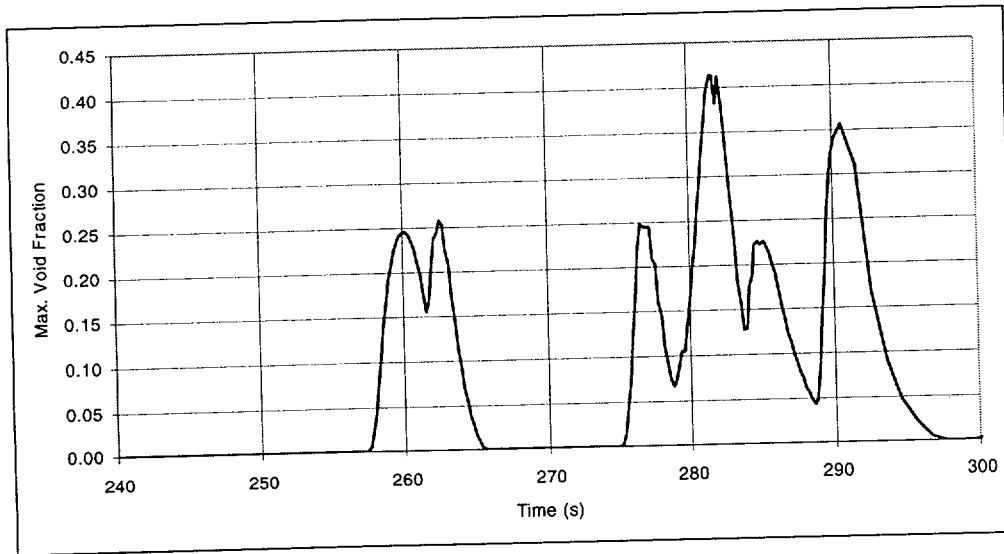


**Figure 3.2.10 Maximum Void Fraction in Case 2**

<b>1</b> 89 30.69	2 90 0.16	3 91 29.5	4 92 0.18	5 93 24.53	6 94 0.16	7 95 36.51	8 96 48.2
	<b>9</b> 105 32.26	10 106 0.17	11 107 29.3	12 108 0.17	13 109 29.25	14 110 0.15	15 111 40.34
		16 121 31.69	17 122 0.18	18 123 30.12	19 124 0.17	<b>20</b> 125 0.14	21 126 39.62
			22 136 24.52	23 137 0.18	24 138 31.73	<b>25</b> 139 26.73	
				26 150 24.89	27 151 0.17	<b>28</b> 152 32.22	
					29 163 24.82		

High Void  
TH Channel  
FA  
Burnup (GWD/T)

Figure 3.2.11 Thermal-Hydraulic Channels with High Void in Case 2

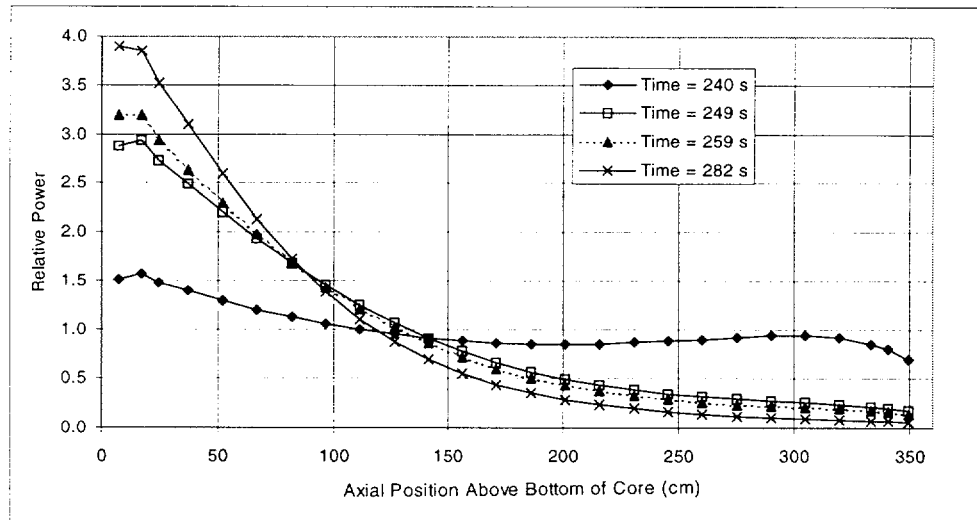


Figure 3.2.12 Axial Power Distribution in Case 2

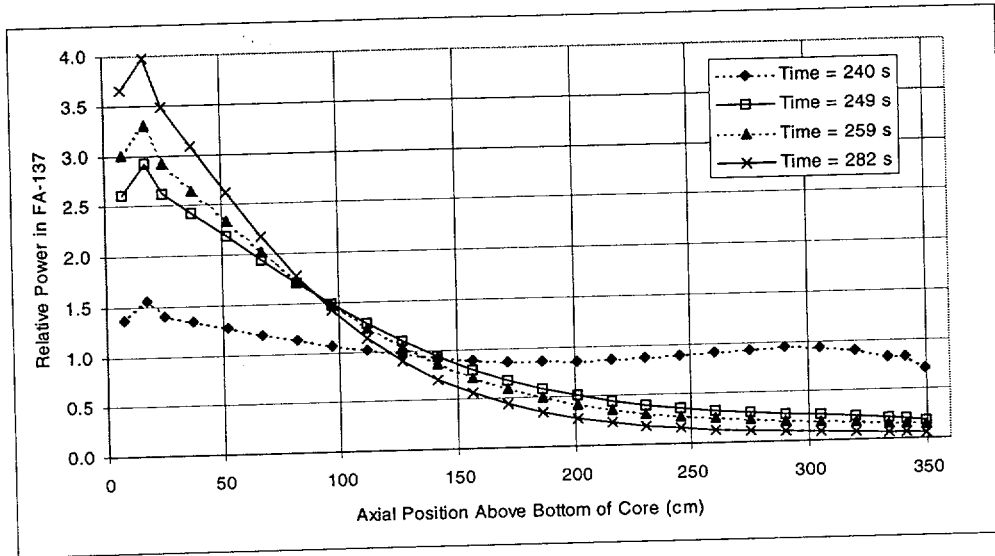


Figure 3.2.13 Axial Power Distribution in FA-137 (TH-23) in Case 2

0.583	1.113	0.669	1.456	0.897	1.207	0.435	0.187
	0.630	1.365	0.947	1.634	0.784	0.809	0.221
		0.960	<b>1.845</b>	1.523	1.418	0.426	0.156
			1.248	<b>1.993</b>	0.866	0.490	
				1.306	<b>1.627</b>	0.453	
					0.882		

Figure 3.2.14 Assembly-Averaged Radial Power Distribution at Time ~ 259 s in Case 2

0.510	0.896	0.670	1.197	0.807	1.031	0.436	0.201
	0.616	1.122	0.881	1.415	0.773	0.822	0.246
		0.879	<b>1.607</b>	1.555	1.329	0.494	0.183
			1.210	<b>1.925</b>	0.986	0.645	
				1.460	<b>2.119</b>	0.663	
					1.191		

Figure 3.2.15 Radial Power Distribution in Axial Plane k=3 (z=17 cm) at Time ~ 259 s in Case 2

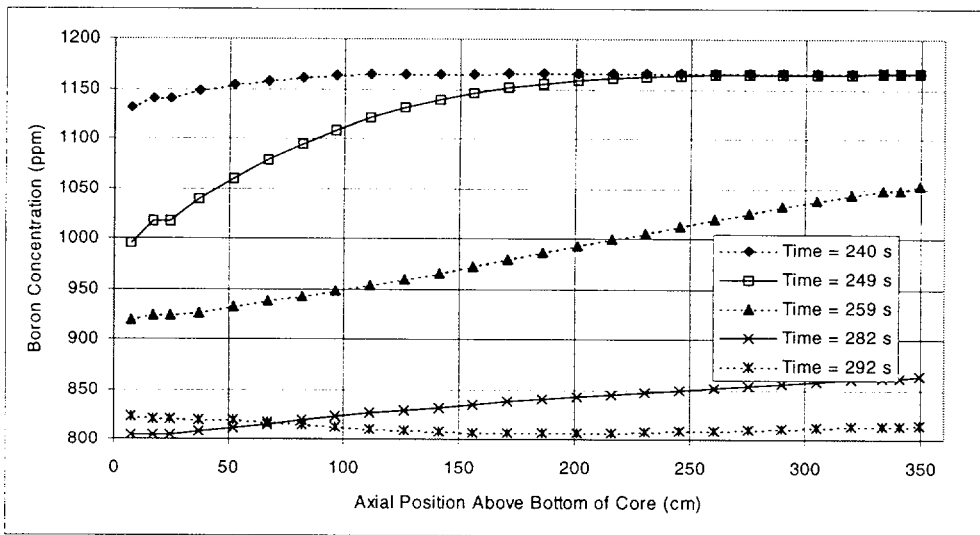


Figure 3.2.16 Plane-Average Axial Boron Distribution in Case 2

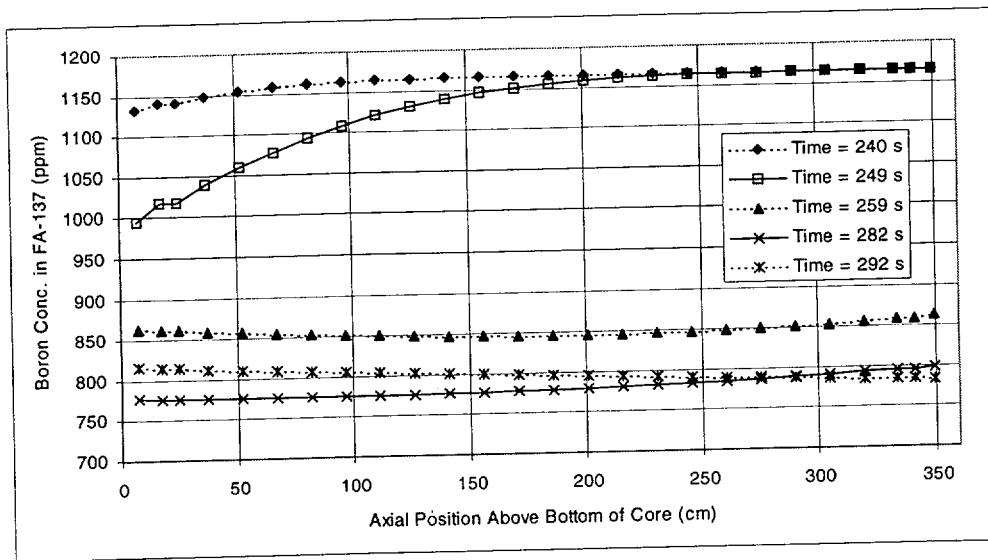


Figure 3.2.17 Axial Boron Distribution in FA-137 (TH-23) in Case 2

894	819	846	798	837	810	912	902
	917	801	825	790	844	837	904
		827	<b>785</b>	787	794	919	902
			800	<b>781</b>	819	924	
				791	<b>780</b>	873	
					805		

Figure 3.2.18 Assembly-Averaged Radial Boron Distribution at Time ~ 282 s in Case 2

621	776	779	776	777	776	938	919
	796	776	776	776	778	777	921
		776	<b>776</b>	776	776	950	918
			776	<b>776</b>	776	796	
				776	<b>776</b>	793	
					776		

Figure 3.2.19 Radial Boron Distribution in Plane k=3 (z=17 cm) at Time ~ 282 s in Case 2

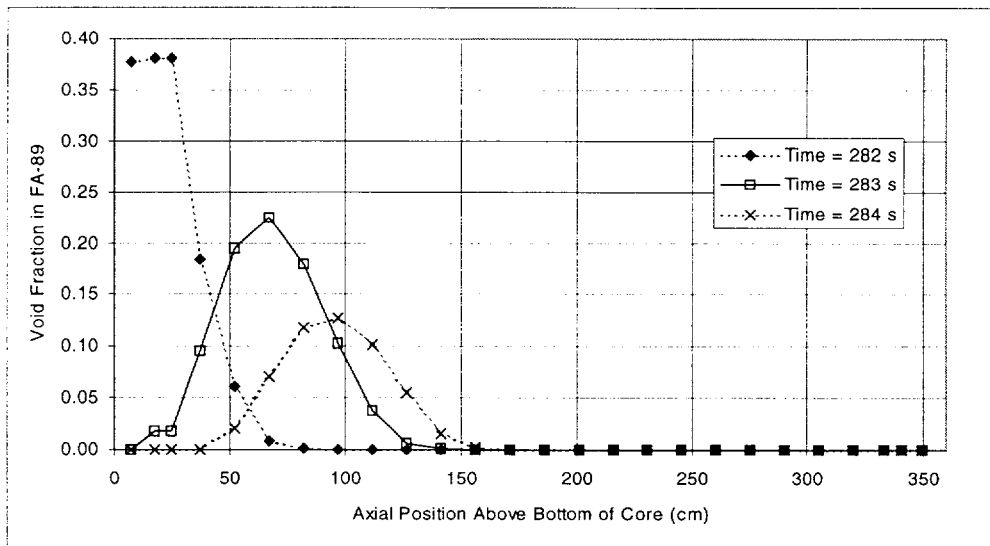


Figure 3.2.20 Axial Void Distribution in FA-89 (TH-01) in Case 2 at Time ~ 282 s

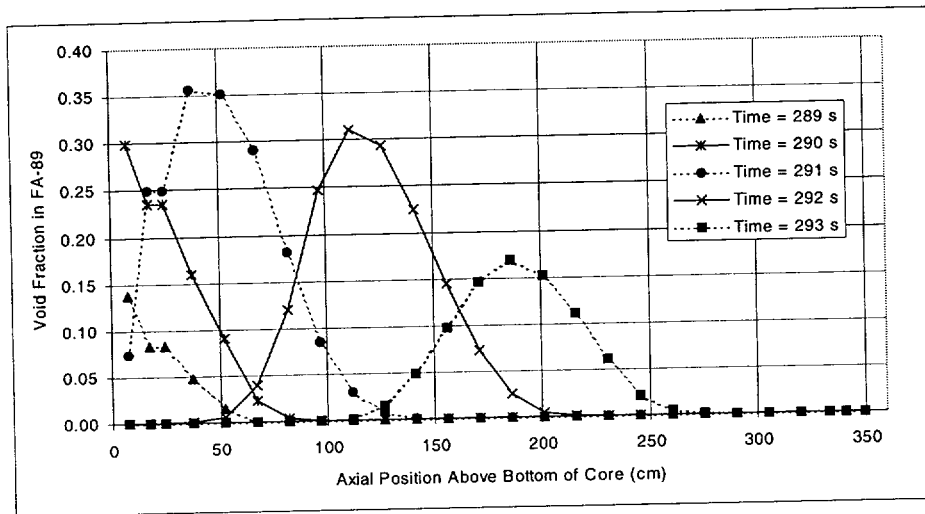


Figure 3.2.21 Axial Void Distribution in FA-89 (TH-01) in Case 2

690	696	697	693	698	696	719	722
	706	694	697	691	698	698	721
		697	<b>688</b>	689	693	718	722
			694	<b>683</b>	697	703	
				692	<b>681</b>	699	
					696		

Figure 3.2.22 Assembly Averaged Radial Coolant Density Distribution at Time ~ 282 s in Case 2

0.880	1.748	1.547	2.228	1.593	1.855	-1.703	-2.293
	-0.363	2.109	1.690	2.527	1.556	1.560	-2.193
		1.675	<b>2.826</b>	2.693	2.326	-1.350	-2.334
			2.159	<b>3.236</b>	1.736	1.785	
				2.480	<b>3.386</b>	1.315	
					1.980		

**Figure 3.2.23 Normalized Mass Flux Distribution in Case 2 at Time ~ 282 s at Inlet Junctions of Core (Mass Flux Average = 105.565 kg/m<sup>2</sup>/s, Total Flow Area = 5 m<sup>2</sup>)**

1.209	1.688	1.481	2.114	1.530	1.782	-1.422	-1.951
	-0.044	2.010	1.627	2.377	1.486	1.501	-1.861
		1.613	<b>2.645</b>	2.524	2.196	-1.109	-1.988
			2.048	<b>3.009</b>	1.668	1.514	
				2.329	<b>3.138</b>	1.263	
					1.884		

**Figure 3.2.24 Normalized Mass Flux Distribution at Time ~ 282 s in Case 2 at Outlet Junctions of Core (Mass Flux Average = 117.525 kg/m<sup>2</sup>/s, Total Flow Area = 5 m<sup>2</sup>)**

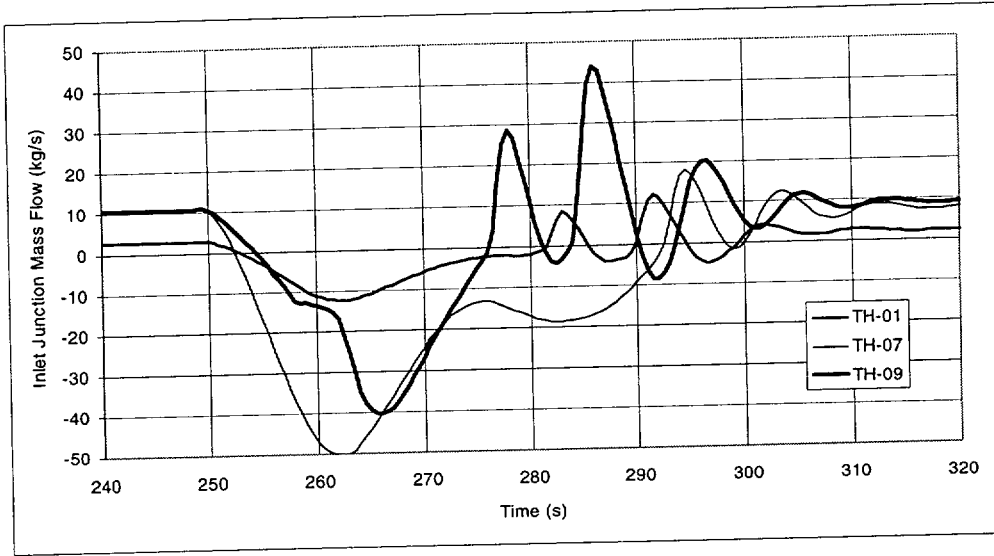


**Figure 3.2.25 Mass Flow in High-Void Channels TH-01, TH-07, TH-09**

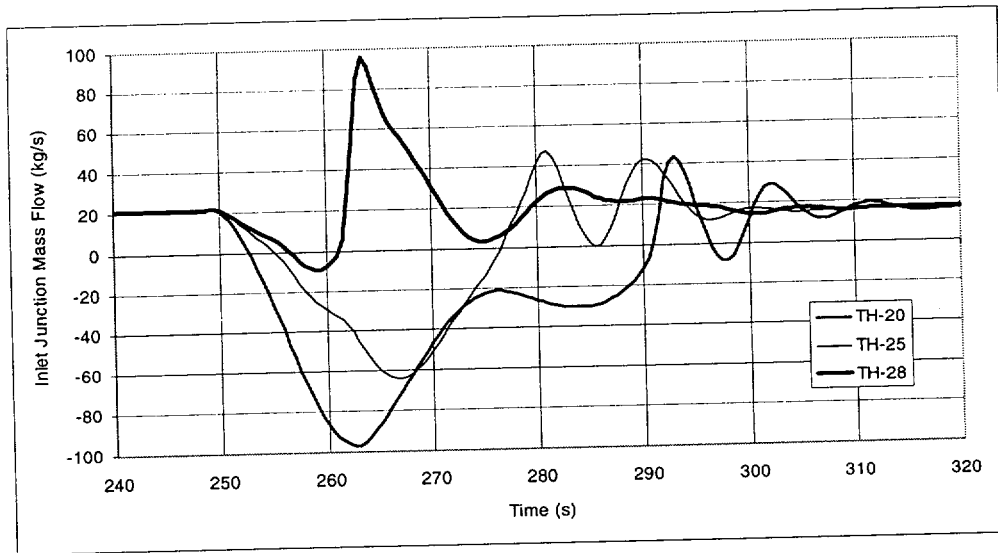


**Figure 3.2.26 Mass Flow in High-Void Channels TH-20, TH-25, TH-28**

### 3.3 Comparisons with B&WOG Results

Because the reactor cores and modeling approaches are different, comparisons between the BNL simulations of the boron dilution event in the TMI-1 and the simulations done for the B&WOG for CR-3 are only modestly quantitative. The B&WOG analysis used a quasi-three-dimensional core thermal-hydraulic model in a stand-alone RELAP5 simulation incorporating a point-kinetics model. In the CR-3 core model, the 12 peak-power assemblies were grouped into a single thermal-hydraulic hot channel, while the other 165 assemblies were lumped together into a single average core channel. The two lumped thermal-hydraulic channels in the B&WOG analysis of the core had 22 axial nodes, and were laterally connected by junctions at each axial node to allow cross flow between the average hot channel and the average core channel. The two core channels were parallel with two additional single channels representing the baffle region and bypass regions of the core, and these were all connected to common mixing volumes at the inlet and exit, which were then connected to single non-mixing volumes representing the lower and upper plena of the reactor. The required input power shape factors and reactivity coefficients for the point-kinetics model were computed separately by the NEMO neutronics code.

In contrast, the BNL analysis used a more detailed three-dimensional coupled neutronics/thermal-hydraulics model with PARCS/RELAP5. Each fuel assembly in the BNL analysis was modeled as a separate, parallel thermal-hydraulic channel. The BNL Case 2 boron dilution transient was set up to more closely approximate the B&WOG simulation, with the core reactivity being close to zero, and the boron deficit relative to the critical concentration for the lower inlet plenum dilution curve being the same.

The B&WOG analysis used the core inlet boron dilution curve instead of the lower inlet plenum curve in their analysis. The boron concentration was assumed to be uniform throughout the core, and its effect was incorporated directly into the point-kinetics model as a time-dependent reactivity change based upon the boron reactivity coefficient. This approach was considered to be conservative. After a one-hour initialization transient was used to bring the CR-3 core to conditions that would represent the restart of natural circulation after a 0.007-ft<sup>2</sup> SBLOCA, the total reactivity and all reactivity components were set artificially to zero, and the simulation was started at the 160-second mark in the 500-second boron dilution event (see Figure 2.7). At 160 s, the core inlet boron concentration is at the critical value (1494 ppm) for the CR-3 PWR at 149 °C and 6.89 MPa with all control rods inserted after operating effectively for 4 days at full power, with no xenon production. With the pre-calculated boron reactivity coefficient (-7.58 pcm/ppm), the boron dilution curve based upon the core inlet resulted in an effective peak boron reactivity component of \$3.44 over 40 s. The CR-3 core took 5 s to go from zero reactivity to prompt-critical. The power peaked at 83%, 6 s after the beginning of the dilution transient. The maximum fuel pellet temperature of 1118 °C was reached after 29 s at 59 cm above the bottom of the core. This corresponded to an enthalpy change of approximately 69 cal/g. Sufficient power generation and heat transfer to the coolant caused sporadic void formation, going as high as 26% in the hot channel at 130 cm above the bottom the core. Voids formed and collapsed in the hot channel every 4 to 5 s for approximately 40 s. Negative Doppler and moderator feedback caused the reactor to go subcritical after 50 s, and the power dropped below 10% after 80 s.

In spite of the modeling differences, reasonable comparisons can be made between the BNL analysis and the B&WOG analysis of the boron dilution event. The time for the core to go from approximately zero to prompt criticality went from 4 to 13 s in going from the BNL Case 1 to Case 2 simulations, bracketing the 5 s value in the B&WOG-AC test. The longer period in Case 2

is attributed to the lower boron dilution rate and the more uniform axial boron concentration distribution before reaching prompt-critical. The BNL analysis modeled spatial boron variations, while the B&WOG analysis did not. The peak power in the BNL analysis was quite comparable (80 and 74 % for Case 1 and 2, respectively, versus 83%), but the pulse width of the first power pulse was shorter (94 and 760 ms versus 1.5 s). The peak fuel pellet enthalpy rise in the BNL analysis (16 and 37 cal/g) was 77% and 46% lower than the B&WOG result (69 cal/g), and the hot spot occurred closer to the bottom of the core (37 and 17 cm versus 130 cm). Although higher voids were found in the BNL Case 2 (over 41% versus 26%), the periods at which voids formed and collapsed were quite similar (approximately 5 s). After reaching prompt critical conditions, Case 1 took 12 s to return permanently to a sub-critical state, whereas Case 2 took 24 s. The B&WOG simulation took 45 s to return to a sub-critical state permanently. The boron was less diluted in Case 1, and there was more negative feedback in Case 2 than in the B&WOG simulation. The power dropped permanently below 10% in Case 1, 9 s after the initial power peak, and in Case 2, 51 s after the initial power peak, whereas in the B&WOG simulation, the power did not drop below 10% until 70 s after the initial peak. Although no evaluation of the DNBR was done by the B&WOG, the BNL results for both Case 1 and Case 2 demonstrated that the DNBR ratio did not get close to a limiting value.

#### 4. CONCLUSIONS AND RECOMMENDATIONS

The main objective of this study was to evaluate the potential for fuel damage in the core of a PWR due to re-criticality caused by boron dilution after a restart of natural circulation following a small break loss-of-coolant accident. Fuel damage may result due to excessive energy deposition, or departure from nucleate boiling. Previous simulations of boron dilution events, although considered conservative, did not give a complete, three-dimensional, time-dependent, coupled neutronics/thermal-hydraulics model of every fuel assembly.

Using modified boron dilution curves, developed earlier for the B&W Owners Group (B&WOG) by Framatome Technologies, as lower inlet plenum boundary conditions, two boron dilution transients were simulated. They were done with a beginning-of-cycle core model of the TMI-1 PWR using the coupled PARCS/RELAP5 neutronics/thermal-hydraulics codes. Due to limitations of the tabulated cross section data base used in the core neutronics model, a minimum moderator coolant temperature of 500 K was used instead of the more probable 422 K. To maintain the same enthalpy subcooling of the coolant at the lower inlet plenum, the pressure during the transient was maintained at 15 MPa, instead of being reduced to the expected 6.6 MPa.

The boron dilution transients caused the core to go above prompt-critical, with peak reactivities and powers as high as 1.02 and 80% of nominal, respectively. The peak enthalpy change in the fuel was found to be 16 and 37 cal/g in the two BNL simulations, which was 77 and 46% lower than the value obtained in the more approximate analysis by the B&WOG. The hottest fuel was found near the bottom of the core in low burn-up, unrodded fuel assemblies near the reflector. Auto-catalytic behavior occurred in the BNL simulations, where natural circulation forces preferentially drove more diluted water through the hotter channels, further increasing the localized relative power levels. For the case with larger boron deficit, the power deposition in the fuel and heat transfer to the coolant were sufficient to cause significant void formation (over 40% void fraction) in a few channels experiencing flow reversal. Competing reactivity components due to changes in moderator density, boron deficit and fuel temperature caused a few modest power fluctuations over a period of ~40 s. The minimum DNBR ratio never dropped below 3.0 during the simulations of the boron dilution event, and so the probability of departure from nucleate boiling is quite low.

In consideration of the maximum fuel pellet enthalpy change, the more approximate model used for the B&WOG study is probably conservative, although it does not properly account for several processes affecting the outcome of a boron dilution event. These include the time-dependent spatial variation of the boron concentration and mixing processes that occur throughout the core and in the inlet and exit plena. As a result, the B&WOG analysis cannot model the auto-catalytic behavior that occurs in unrodded low-burnup fuel assemblies near the reflector. It also does not accurately account for the feedback from moderator density and fuel temperature changes which are dependent on complex spatial distributions.

The question of the potential for fuel damage due to departure from nucleate boiling in the boron dilution event may require a finer computational mesh for both the neutronic and thermal-hydraulic calculations, or perhaps even a fuel assembly sub-channel calculation. In addition, since the current PARCS/RELAP5 model of the TMI-1 core does not permit cross-flow between fuel assemblies (except at the inlet and exit plena), additional uncertainty is added to the results.

Another issue to consider is the validity of the shape and magnitude of the boron dilution transient generated by a SBLOCA in the B&W PWR. The boron dilution curves computed for the CR-3

reactor were adapted for the BNL analysis of the TMI-1 core; however, a separate system analysis of the TMI-1 plant in the event of a SBLOCA may yield boron dilution transients that are substantially different, and this will affect the subsequent transient neutronics/thermal-hydraulics simulations. In general the ability to model mixing limits the accuracy of the inlet boron concentration calculated for use in the core analysis.

The tabulated two-group cross section data base for the homogenized fuel assemblies used in the neutronics model of the TMI-1 core should be extended for future analyses to include the more extreme conditions that would be experienced during boron dilution events, especially low coolant temperatures and high boron concentrations. Tabulated cross section data should be generated for coolant temperatures as low as 300 K, for Doppler fuel temperatures ranging from 300 to 2300 K, and for boron concentrations as high as 2500 ppm. A larger data base will help avoid the errors and uncertainty that are incurred by extrapolating data outside the existing range of applicability.

## 5. REFERENCES

1. The B&W Owners Group Analysis Committee, "Evaluation of Potential Boron Dilution Following Small Break Loss-of-Coolant Accident," Report 77-5002260-00 , Framatome Technologies, Lynchburg, VA, September 1998.
2. B. Dunn and N.H. Shah, "Evaluation of Potential Boron Dilution Following Small Break Loss-of-Coolant Accident, Final Report" Report 47-5006624-00 , Framatome Technologies, Lynchburg, VA, c 2000.
3. Generic Safety Issue No. 185, "Control of Recriticality Following Small-Break LOCAs in PWRs," U.S. Nuclear Regulatory Commission, July 7, 2000.
4. J.E. Rosenthal, "Task Action Plan for Resolving Generic Safety Issue 185: 'Control of Recriticality Following Small-Break LOCAs in PWRs,'" Memo to F. Eltawila, U.S. Nuclear Regulatory Commission, March 19, 2001.
5. H.G. Joo et al., "PARCS: A Multi-Dimensional Two-Group Reactor Kinetics Code Based on the Non-linear Analytic Nodal Method," PU/NE-98-26, Purdue University, School of Nuclear Engineering, September 1998.
6. INEL and EG&G, Idaho Falls, Idaho, "RELAP5/MOD3 Code Manual," NUREG/CR-5535, U.S. Nuclear Regulatory Commission, Washington, D.C., March 1998.
7. K.N. Ivanov et al., "PWR Main Steam Line Break (MSLB) Benchmark; Volume I: Final Specifications," NEA/NSC/DOC(99)8, U.S. Nuclear Regulatory Commission and OECD Nuclear Energy Agency, April 1999.
8. N.K. Todorova and K.N. Ivanov, "Project Report on Task 1 of BNL Sub-contract Core Model - PARCS/RELAP5," Nuclear Engineering Program, Pennsylvania State University, August 2000.
9. D.J. Diamond et al., "Intercomparison of Results for a PWR Rod Ejection Accident," Proceedings of the Twenty-Seventh Water Reactor Safety Information Meeting, October 1999, NUREG/CP-0169, U.S. Nuclear Regulatory Commission, March 2000.
10. A. Avvakumov, V. Malofeev, and V. Sidorov, "Analysis of Pin-by-Pin Effects for LWR Rod Ejection Accident," Russian Research Centre - Kurchatov Institute, NUREG/IA-0175, U.S. Nuclear Regulatory Commission, March 2000.
11. A. Avvakumov, Russian Research Centre - Kurchatov Institute, Private Communication to David Diamond, Brookhaven National Laboratory, February 28 and July 4, 2001.
12. A. Avvakumov, Russian Research Centre - Kurchatov Institute, Private Communication to Blair P. Bromley, Brookhaven National Laboratory, December, 2001.